

AD-A138 843

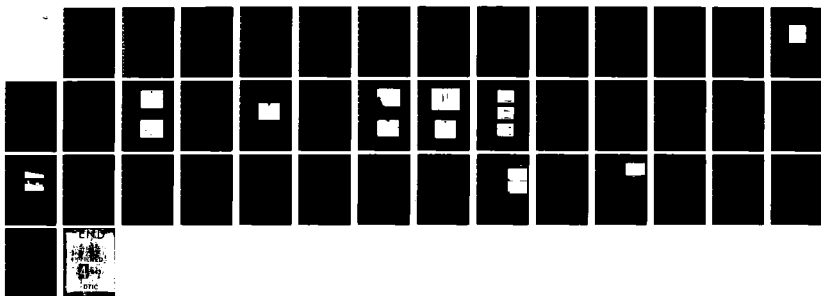
REAL-TIME IMPLEMENTATION OF NONLINEAR OPTICAL  
PROCESSING FUNCTIONS(U) HUGHES RESEARCH LABS MALIBU CA  
B H SOFFER DEC 83 AFOSR-TR-84-0141 F49620-81-C-0086

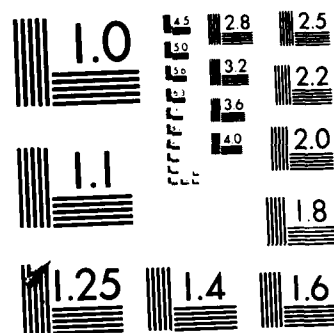
1/1

UNCLASSIFIED

F/G 20/6

NL





MICROCOPY RESOLUTION TEST CHART  
NATIONAL BUREAU OF STANDARDS-1963-A

4

AD A138843

## REAL-TIME IMPLEMENTATION OF NONLINEAR OPTICAL PROCESSING FUNCTIONS

B.H. Soffer

Hughes Research Laboratories  
3011 Malibu Canyon Road  
Malibu, CA 90265

December 1983

F49620-81-C-0086

Annual Technical Report

15 June 1982 through 15 June 1983

*This manuscript is submitted for publication with the understanding  
that the United States Government is authorized to reproduce and dis-  
tribute reprints for governmental purposes.*

Prepared For

AIR FORCE OFFICE OF SCIENTIFIC RESEARCH

Bolling Air Force Base

Washington, DC 20332

DTIC

MAR 8 1984

The views and conclusions contained in this document are those of the author and should not be interpreted as necessarily representing the official policies or endorsements either expressed or implied of the Air Force Office of Scientific Research or the U.S. Government.

DTIC FILE COPY

Approved for public release;  
distribution unlimited.

84 03 06 016

UNCLASSIFIED

SECURITY CLASSIFICATION OF THIS PAGE (When Data Entered)

REPORT DOCUMENTATION PAGE		READ INSTRUCTIONS BEFORE COMPLETING FORM
1. REPORT NUMBER <b>AFOSR-TR- 84-0141</b>	2. GOVT ACCESSION NO. <i>AD 1155 175</i>	3. RECIPIENT'S CATALOG NUMBER
4. TITLE (and Subtitle) Real-Time Implementation of Nonlinear Optical Processing Functions		5. TYPE OF REPORT & PERIOD COVERED Annual Technical Report 15 June 1982 - 15 June 1983
7. AUTHOR(s) B.H. Soffer		6. PERFORMING ORG. REPORT NUMBER
9. PERFORMING ORGANIZATION NAME AND ADDRESS Hughes Research Laboratories 3011 Malibu Canyon Road Malibu, CA 90265		8. CONTRACT OR GRANT NUMBER(s) F49620-81-C-0086
11. CONTROLLING OFFICE NAME AND ADDRESS		10. PROGRAM ELEMENT, PROJECT, TASK AREA & WORK UNIT NUMBERS <i>2305/81</i> <i>61102F</i>
14. MONITORING AGENCY NAME & ADDRESS (if different from Controlling Office) Air Force Office of Scientific Research / <i>NE</i> Bolling Air Force Base Washington, DC 20332		12. REPORT DATE December 1983
		13. NUMBER OF PAGES <i>43</i>
		15. SECURITY CLASS. (of this report) Unclassified
		15a. DECLASSIFICATION/DOWNGRADING SCHEDULE
16. DISTRIBUTION STATEMENT (of this Report) This manuscript is submitted for publication with the understanding that the United States Government is authorized to reproduce and distribute reprints for governmental purposes. <i>Approved for public release; distribution unlimited.</i>		
17. DISTRIBUTION STATEMENT (of the abstract entered in Block 20, if different from Report)		
18. SUPPLEMENTARY NOTES Research sponsored by the Air Force Office of Scientific Research (AFSC), under Contract F49620-81-C-0086. The United States Government is authorized to reproduce and distribute reprints for governmental purposes notwithstanding any copyright notation hereon.		
19. KEY WORDS (Continue on reverse side if necessary and identify by block number) Optical signal processing, optical data processing, signal processing, data processing, liquid crystal devices.		
20. ABSTRACT (Continue on reverse side if necessary and identify by block number) Optical data processing has not yet achieved its potential of increased capacity and speed compared with conventional electronic techniques, primarily for lack of a practical real-time image modulator, and because optical techniques have been almost exclusively limited to linear operations. The continuing research outlined in this report attacks these issues by studying the implementation of real-time nonlinear parallel-processing techniques. The various implementations studied in this program all employed real-time liquid-crystal light valves developed and specially modified for these tasks by Hughes Research		

UNCLASSIFIED

SECURITY CLASSIFICATION OF THIS PAGE (When Data Entered)

UNCLASSIFIED

SECURITY CLASSIFICATION OF THIS PAGE(When Data Entered)

Laboratories. One approach we investigated early in the program was to modify and characterize the twisted-nematic liquid-crystal (LC) devices, and then use them in a coherent optical data-processing apparatus using special half-tone screen masks, custom designed for special functions at USC in a cooperative effort under an AFOSR grant. Using the half-tone mask technique, we demonstrated logarithmic nonlinear transformation, permitting us to simplify multiplicative images and perform homomorphic filtering. Furthermore, a novel analog-to-digital converter based on a modified pure birefringence LCLV was developed. It can perform real-time parallel processing using incoherent light, and it promises high data throughput rates. In addition, a novel device that converts light intensity variations to LC grating period variations was fabricated, and is currently being evaluated and improved. This device permits nonlinear functions to be implemented directly without the need for specially made half-tone masks. Besides nonlinear analog functions, this variable grating mode (VGM) device has demonstrated the capability of performing digital logic. Logical functions are merely special cases of nonlinearities. In this period we report a novel technique for spoiling the long-range order in the VGM substrate to show a remarkable improvement in the temporal response. An alternative to the VGM device, which retains the essential optical processing features, is described.



UNCLASSIFIED

SECURITY CLASSIFICATION OF THIS PAGE(When Data Entered)

# LIST OF ILLUSTRATIONS

FIGURE		PAGE
1.	Design of holographic grating substrate.....	8
2.	VGM domains aligned perpendicular to the horizontal.....	9
3.	Apparatus for studies of the dynamics of VGM response.....	10
4.	VGM temporal response; +20 to +30 V dc, 1 $\mu$ m grating substrates, 500 msec/cm.....	12
5.	VGM temporal response to +30 + 40 V dc, 1 $\mu$ m grating substrates, 2 sec/cm.....	12
6.	VGM temporal response; +30 to -40 V dc, 1 $\mu$ m grating substrates, 300 msec/div.....	14
7.	VGM domains in cross-rubbed PVA cell, 180X.....	16
8.	VGM temporal response; -40 to +60 V dc,.....	16
9.	SEM photograph of 0.4 $\mu$ m holographic grating of ITO on glass.....	17
10.	VGM temporal response; +40 to +30 V dc, 0.4 $\mu$ m grating substrates perpendicularly disposed, 2 sec/div.....	17
11.	VGM frequency response; -40 to +20 V, 1 $\mu$ m grating substrates, 1 Hz to 30 Hz sweep.....	18
12.	V-shaped grooves with (111) walls are produced by etching in (100) silicon slice.....	23
13.	Blaze angle is determined by inclination angle between the silicon surface and the (111) plane.....	23
14.	Short period grating in single crystal silicon.....	24

AIR FORCE OFFICE OF SCIENTIFIC RESEARCH (AFSC)  
 NOTICE OF REVISION TO DTIC  
 This document has been reviewed and is  
 approved for release under E.O. 13526-12.  
 Distribution is unlimited.  
 MATTHEW J. KERLEY  
 Chief, Technical Information Division

## SECTION 1

### INTRODUCTION

For the past two decades optical data processing (ODP) has promised a vast increase in processing capacity and speed over conventional electronic techniques. This promise has never been fulfilled for several reasons, most notably because of the lack of a practical real-time image modulator, or light valve, and because optical techniques were almost exclusively limited to linear operations. These restrictions have been removed by the development of the liquid-crystal light valve (LCLV) by Hughes Research Laboratories (HRL), and by nonlinear parallel-processing techniques developed by the University of Southern California (USC). Thus, it is important to determine how successfully non-linear parallel-processing techniques can be implemented in real time with the various LCLVs.

The implementation and evaluation of these techniques have a direct relationship to current Air Force technology. Pertinent Air Force interests include multidimensional real-time signal and image processing with varied applications, including nonlinear filtering for trajectory control and guidance, "smart" sensing, picture processing, and bandwidth compression. These technologies could benefit substantially from the increased processing capacity and speed that the proposed research may yield.

Here we describe nonlinear optical transformation methods and the motivation for studying a real-time application of those techniques. In Section 2 we describe the progress made during the current program year. The HRL-developed photactivated twisted-nematic LCLV, the variable grating mode (VGM) LCLV modification and its system configuration for optical processing, and optical logical operation has been described in previous reports. A study of the dynamic performance of the VGM LCLV has

been performed in this period using a novel technique to reduce the time of VGM domain formation. Empirical modeling of the VGM effect has also been performed.

The implementation and evaluation of these techniques has a direct relationship to Air Force interests in the multidirectional processing of real-time signals and images, with applications including nonlinear filtering for guidance and trajectory control, smart sensing, picture processing, and bandwidth compression. These technologies could benefit substantially from the increased processing capacity and speed that these techniques may yield.

Until now, specified nonlinear operations have been performed only with great difficulty. Coherent optical techniques are essentially restricted to linear operations. Digital processing to produce nonlinear transformations is possible, but only in a slow, serial fashion. Certain nonlinearities can be produced by special photographic techniques, but the speed, accuracy, reproducibility, and dynamic range of these techniques are limited.

We have been pursuing different tasks to attempt to overcome these shortcomings. The first made use of special half-tone screens to modulate the input image in conjunction with coherent optical processing to desample in the Fourier plane. This technique has made it possible to implement nonlinear effects when higher orders of the half-tone diffraction pattern are examined by spatial filtering. Sawchuk and Dashiell of USC have shown, using specially fabricated half-tone screens, how a very wide class of two-dimensional point nonlinear functions can be implemented with a large dynamic range as a function of screen design and diffraction order. The nonlinearities can be continuous or discontinuous. Operations such as taking logarithms, exponentiation, level slicing, intensity bandstopping, and histogram equalization can be performed. We have expanded the half-tone screen technique by substituting a real-time

photo-modulated LCLV for the static photographic recording medium, and we have successfully demonstrated a logarithmic nonlinear transformation using this technique. This transformation is useful for homomorphic-filtering applications as we have demonstrated. In cooperation with USC, we have also studied the performance potentials and limitations of this implementation and how to iteratively modify and improve the LCLV and half-tone masks.

A second general method which we are presently studying also overcomes the limitations of serial or photographic processing; it employs, in one realization, a liquid-crystal effect - VGM - that can, when incorporated into a new type of photoconductive structure, automatically map image intensity variations into positions in Fourier space. Filtering and reconstructing can then yield many desired nonlinear transformations of the image without the need for specially constructed half-tone masks. A new additional parameter, the intensity, has thus been made available for optical image and data processing. Recognizing that logical operations are merely a special case of nonlinear operations, we have demonstrated a unique and highly advantageous optical computing scheme using the VGM technique. The VGM device is still in an early stage of development and much material research and device development is still needed to make it into a practical, real-time, reliable optical image modulator. This work is still continuing. Alternative practical realizations of intensity to positional mapping are also being studied that may overcome some of the shortcomings of VGM, yet retain the great flexibility offered by intensity-to-positional coding.

## SECTION 2

### PROGRESS DURING CURRENT YEAR

During this program year, we pursued several tasks which aimed at further improving our understanding of the VGM effect and at developing a more practical VGM photoactivated light valve device. In the VGM effect, certain liquid-crystal elements exhibit a phase grating whose local period is proportional to the locally applied voltage. When incorporated into a light valve structure along with a photoconductive layer, local variations in the spatial distribution of light signal or image intensity are converted into local variations in grating period. In the Fourier transform plane, a new parameter - the intensity - is coded into the spatial distribution in a way that allows great freedom to perform nonlinear optical data and image processing, and to perform optical computations as well. In this period, we continued to examine many aspects of the device, including the temporal dynamic properties of the light valve using novel schemes to increase the speed of response. The detailed optical polarization properties of the VGM diffraction patterns were also studied with the goal of completing the modeling of the molecular configuration of VGM. We also studied alternative schemes to the VGM wherein the main feature of converting intensity variations to positional variations would be included along with the desired faster time response characteristics.

#### A. IMPROVED VGM RESPONSE TIME

At the end of the last period we began a study which showed promise of improving the VGM response time by spoiling the long range order of the periodic domains. In this sub-section we will review these results and discuss our progress during this year.

From the device standpoint, the VGM response times, as we have noted before, are too slow for many applications. It would be desirable to have responses compatible with TV frame rates or faster, on the order of tens of milliseconds. In this section we describe a novel approach to, and some preliminary results for, achieving faster dynamic response. It is based on the intuitive notion that the VGM domains evolve slowly in time, both along the domain direction and in the perpendicular direction.

There is some visual evidence for the slow evolution of the domains. When the voltage is changed in a VGM cell, say to a slightly higher value, under the polarizing microscope one can see the new additional lines coming into the field of view. New lines form by "unzipping" one or more of the numerous fork-shaped dislocations which occur throughout the area of the VGM structure. The unzipping process typically traverses  $\sim 20$   $\mu\text{m}$  at a velocity on the order of magnitude of 10  $\mu\text{m}/\text{sec}$ .

It seemed possible that if the length of the VGM grating domain could be shortened radically so that the unzipping would not have to travel far, that the time of formation of the new VGM steady state could be shortened. One way to cover a two-dimensional area with short VGM domains would be to have the longer domains interrupted by a fixed set of parallel interruptions perpendicular to the length of the domains. The interruption would have to present a strong electrical and/or mechanical perturbation.

We constructed a special cell with one narrow 1-mm groove parallel and another perpendicular to the VGM domains. No difference in response times was noted between these grooves, nor between the grooves and the normal large area VGM cell geometry.

Next we fabricated a set of holographically produced gratings with a one thousand times smaller, 1  $\mu\text{m}$  period. These gratings were formed on ITO coated glass substrates etched through the conductive coatings. The conductive strips were all

electrically connected at one edge. The design of the substrate is shown in Figure 1. Two orthogonal gratings were put on each substrate so that both parallel and perpendicular opposing electrode gratings could be configured in the complete liquid crystal sandwich cell structure. This assured that both these arrangements, and the grating-free areas as well, could all be studied under the same conditions of thickness, temperature impurities, and aging.

The VGM domains in a working cell 6  $\mu$ m thick with 20 V-dc applied are shown in Figure 2. The domains are perpendicular to the two 1-  $\mu$ m holographic gratings. In the photograph, that grating cannot be seen, and only large occasional defects along the direction of the grooves show up. What is noteworthy in this typical photograph is the large number of forked dislocations, as compared with a cell made of normal substrates without any gratings. The domains, however, are not merely 1  $\mu$ m long (the period of the grating), but typically extend to  $\sim 10$   $\mu$ m in length. In a typical cell without gratings the domains may extend several millimeters before forking.

The LC mixture, Merck NPV, was aligned perpendicular to the direction of the grooves of the holographic grating in those experiments that we will report on here. In another set of experiments with the alignment parallel to the grooves, no significant effects were noted.

The temporal response characteristics proved to be complex and impossible to describe merely with a single set of characteristic rise and decay times. The responses are non-exponential and multiprocess with a pronounced memory or hysteresis. There is also a secular degradation in response. All of these complexities remain to be analyzed.

The apparatus shown in Figure 3 was employed to perform the response time measurements. The measurements were taken on the first order diffracted light from the VGM cell. The diffracted spot of the laser beam was from 3 to 5 mm in diameter at the detector 20 cm from the LC plane. The detector was positioned

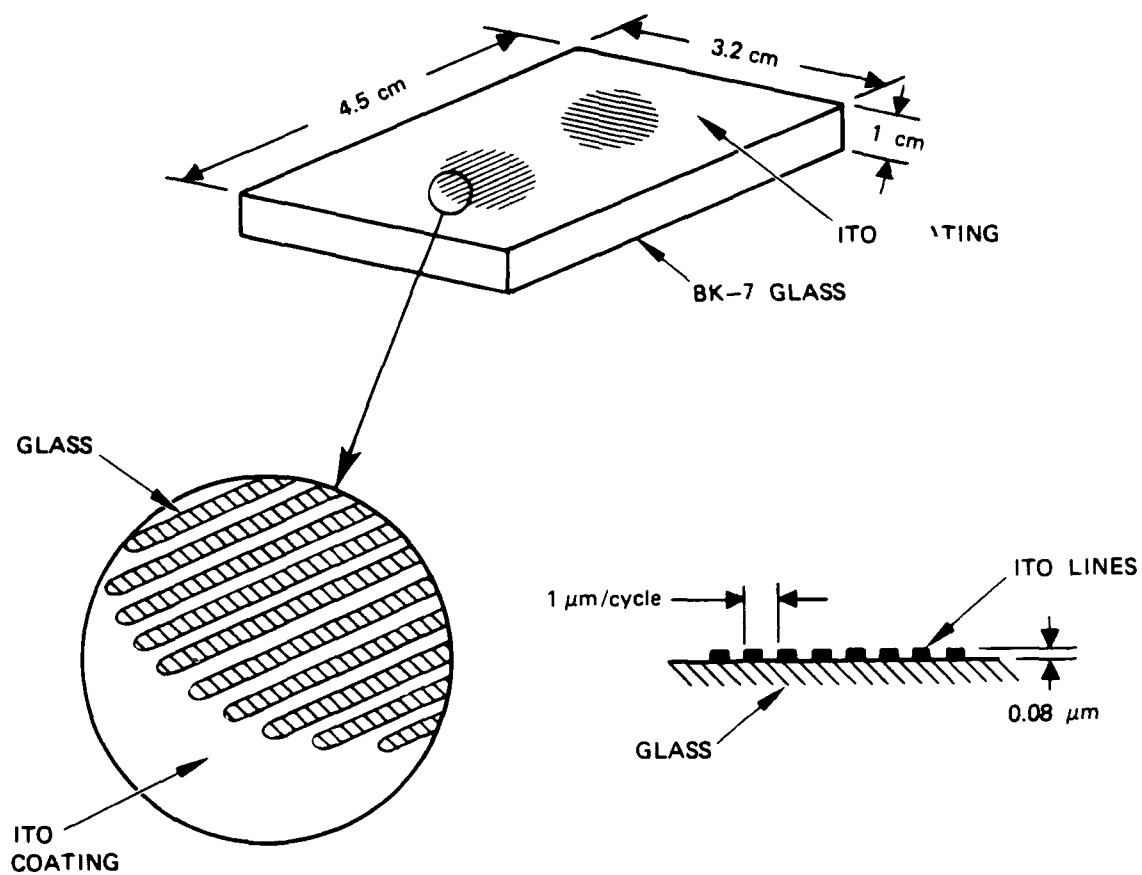


Figure 1. Design of holographic grating substrate.

12545-1

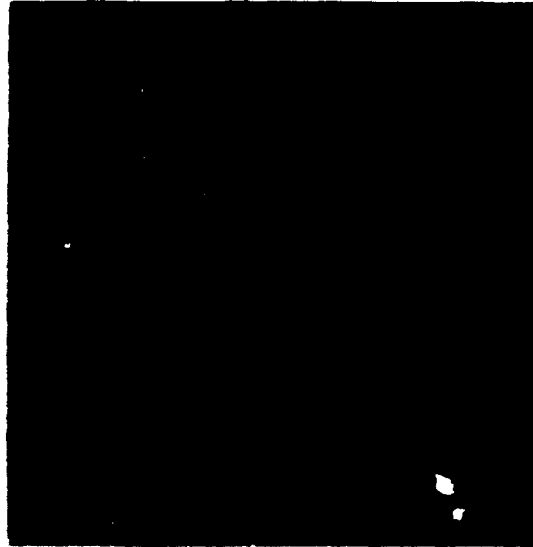


Figure 2. VGM domains aligned perpendicular to the horizontal; 1  $\mu\text{m}$  holographic grating in a 6- $\mu\text{m}$  thick cell with 200 V DC applied

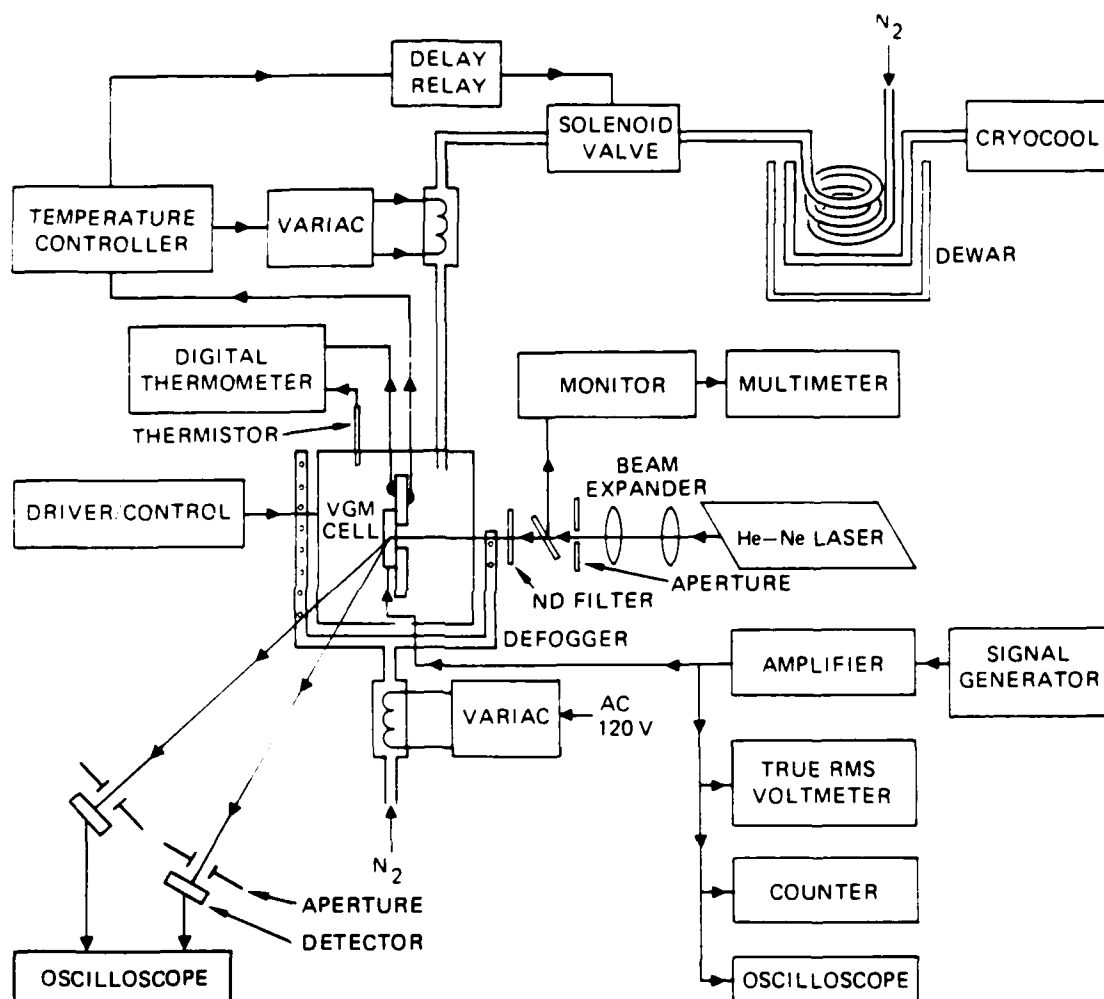


Figure 3. Apparatus for studies of the dynamics of VGM response.

in each experiment at the angle corresponding to the steady state diffraction angle for the particular field applied. A mask was positioned in front of the detector to give an angular resolution of 1 mm at 20 cm from the VGM cell plane.

To measure the temporal response of this cell, the voltage on the cell was repetitively switched from one dc value to another in a rectangular wave pattern. One detector was placed at each of the diffraction positions appropriate for each voltage. The outputs of these detectors were displayed on dual traces of an oscilloscope.

For example, in Figure 4 the top trace records the output of the detector placed at the 30-V diffraction position, while the bottom trace simultaneously records the output of the detector at the 20-V diffraction position as the voltage is repetitively switched from 20 to 30 V in a 2-sec period. The motion of the diffracted light beam from one detector to the other is complex. Not only does the beam travel from one detector to the other, but it also undergoes a reformation and condensation as it approaches steady state, making the temporal response very complicated, as can be seen from the oscilloscope traces. There is also a sudden flash of light, largely centered around the current position, whenever the voltage is switched. This flash shows up as a strong spike on the traces. From Figure 4 we estimate the rise time to be  $600 \pm 200$  msec and the delay time is now only in the tens of milliseconds! In Figure 5 the cell was refilled and traces were recorded from 30 to 40 V. The top trace corresponds to 40 V. Here the rise times were on the order of 100 msec, but the decay times were 600 and 1,700 msec, respectively, for 30 and 40 V. This was clearly not a reproduction of the remarkably rapid decay observed in Figure 4. At this stage in our experiments, we have been able to reproduce the fast performance only from time to time and in only certain of the cells. However, we are greatly encouraged to have seen such significant improvement in temporal response using this new technique. For example, after the gradual deterioration in VGM,

12545-2

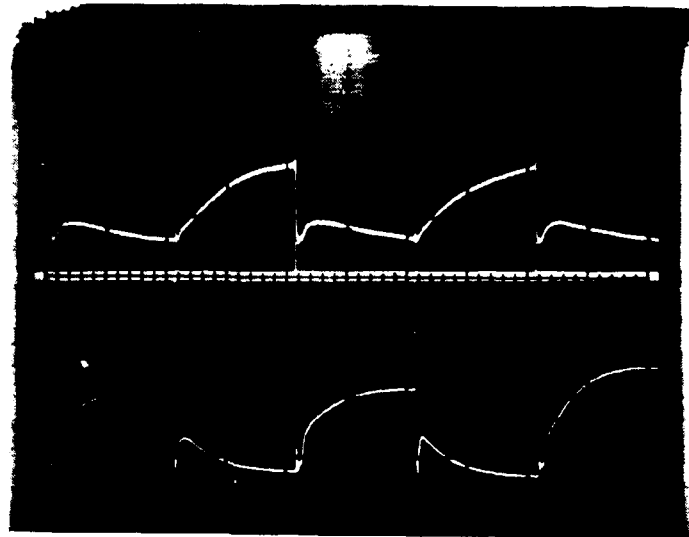


Figure 4. VGM temporal response; +20 to +30 V dc, 1  $\mu$ m grating substrates, 500 msec/cm.

12545-3

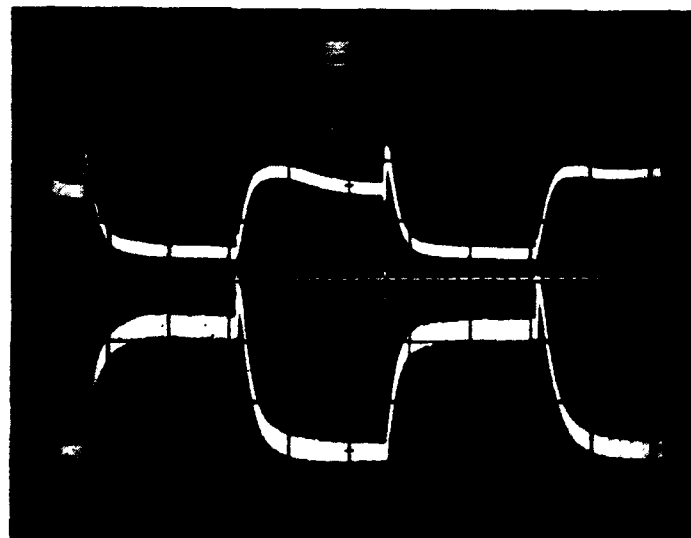


Figure 5. VGM temporal response; +30 to +40 V dc, 1  $\mu$ m grating substrates, 2 sec/cm.

performance of the particular cell studied in Figures 4 and 5 (noted by higher thresholds and increasing conductivity) could no longer be tolerated and the cell was refilled. The decay times were four times slower than the original values. Upon a later second refilling, the times were even slower. This phenomenon is not yet understood.

Next, quasi-ac experiments were tried. If operational, ac would avoid electrochemical poisoning of the liquid crystal. Switching from the same positive to negative voltage values, e.g., +20 V to -20 V in square wave fashion also produced fast decay times of the order of 50 msec and rise times of the order of a second. But as the diffraction angle is the same for the positive as for the negative voltage, and since there is some memory of previous states at the switching times we employed, we abandoned that choice of equal voltage as being misleading.

To take advantage of quasi-ac and yet have more meaningful temporal response measurements, we repetitively performed switchings from +30 to -40 V. Figure 6 illustrates the VGM response of a 1  $\mu$ m holographic grating cell. It should be noted that unless otherwise stated the configuration normally employed is with both electrode and counter electrode gratings parallel to each other. In the top trace the rise time from +30 to -40 V is 300 msec and the decay time  $\approx 10^1$  msec. In the lower trace, measured on the second detector, the rise time from -40 to +30 is 1 sec and the decay time from +30 to -40 is  $\approx 50$  msec. The asymmetry in rise times is not understood.

The production of holographic gratings is time consuming and subject to many difficulties and failure modes in the exposure and etching phases. It seemed that it might be possible to spoil the long range order in the VGM domains by a simpler method: by producing linear, randomly spaced scratches on the substrate surface.

One method of liquid crystal alignment, often used for immediate results, is rubbing. The substrate is rubbed with coarse material, perhaps diamond paste, to effect a quasi-linear pattern of

12778-1

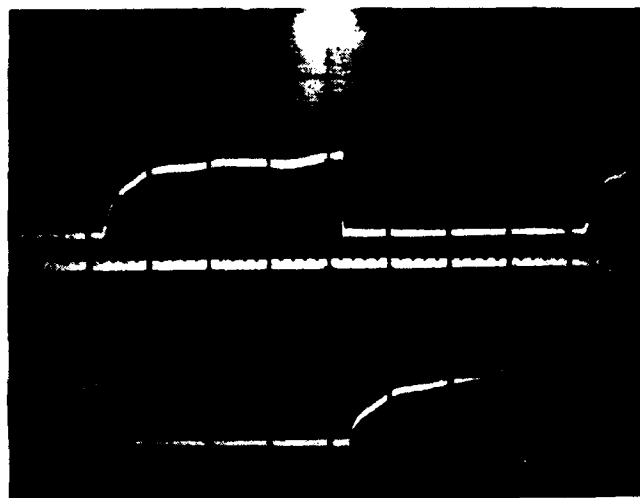


Figure 6. VGM temporal response; +30 to -40V dc,  
1  $\mu$ m grating substrates, 300 msec/div.

surface forces which align the liquid crystal. There is no definite period in these linear scratches. They are randomly spaced. We first rubbed the surface in one direction and then cross-rubbed it in the orthogonal direction. The liquid crystal successfully aligned in the last direction that was rubbed, but the underlying cross-rubbing seemed to achieve the desired effect of breaking up the long range VGM domain order. This can be seen in Figure 7, a polarizing microscope photograph of a cross-rubbed PVA substrate cell spaced at 6  $\mu\text{m}$  and filled with Merck NPV with 50 V dc applied. The long range order is clearly spoiled. The temporal behavior of this cell is shown in Figure 8. The top trace -40 to +60 V shows a rise time of 1.9 sec and decay time of  $\approx 10^1$  msec. Even this crude technique has significantly reduced the response time of the VGM device!

A set of 0.4  $\mu\text{m}$  holographic gratings was fabricated and tested. This period is significantly smaller than the typical VGM instability period and it was unclear whether, for best results in improving the response time, the grating period should be larger or smaller than the VGM period. A scanning electron microscope photograph of the 0.4- $\mu\text{m}$  grating of ITO on glass at 40,000 diameters is shown in Figure 9. The results with this grating have not been as dramatic as with the 1  $\mu\text{m}$  grating, but a significant improvement over no grating at all was still observed. In Figure 10 we display the results for perpendicularly disposed grating electrodes and for +40 to +30 V dc. The rise and decay times are  $\sim 400$  msec. This was typical of the usual grating arrangement as well.

A 6- $\mu\text{m}$  set of holographic grating substrates were fabricated into VGM cells and evaluated. This 6- $\mu\text{m}$  period is somewhat below the typical period of the normal VGM phenomena. With these substrates we could not produce clear VGM phenomena. The diffraction was extremely smeared and confused.

To illustrate the frequency response of the VGM phenomena in the 1  $\mu\text{m}$  grating cells, we show in Figure 11 (a), (b), and

12778-2



Figure 7. VGM domains in cross-rubbed PVA cell, 180X.

12278-3

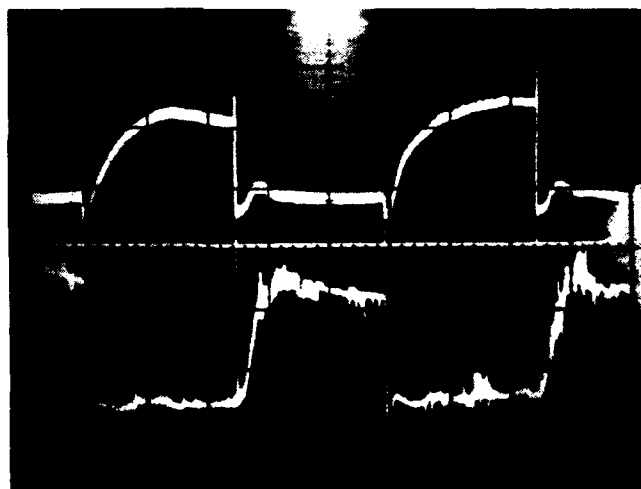


Figure 8. VGM temporal response; -40 to +60 V dc, cross-rubbed PVA substrates. 2 sec/div.

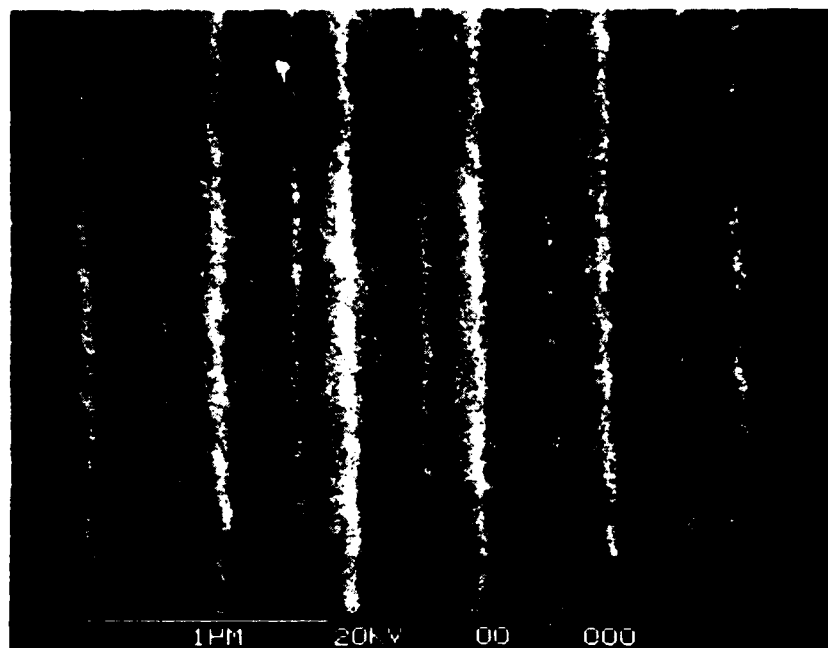


Figure 9. SEM photograph of  $0.4\ \mu\text{m}$  holographic grating of ITO on glass.

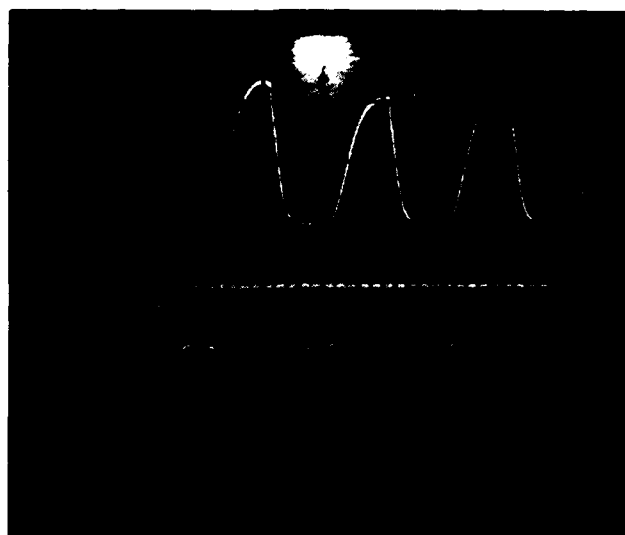
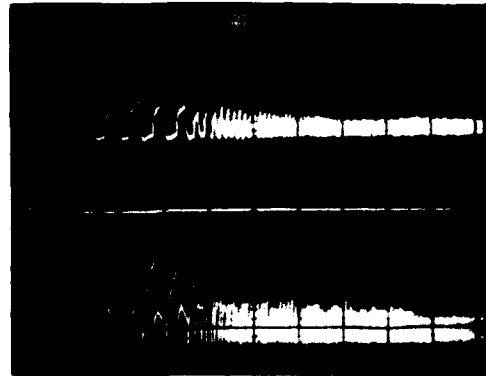
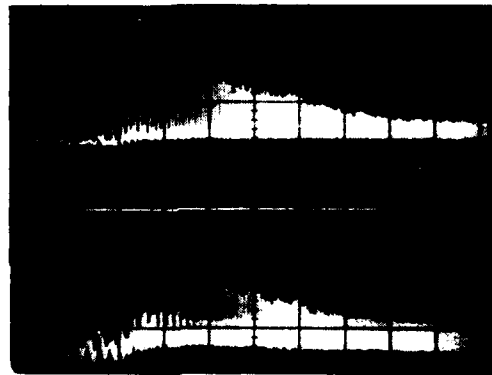


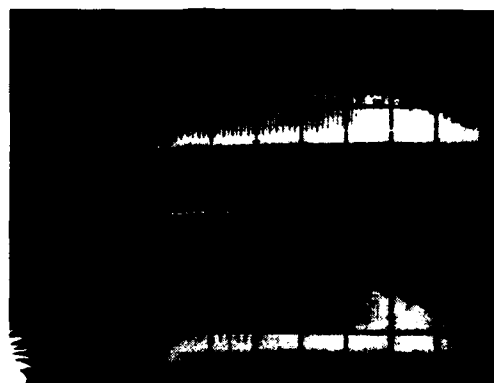
Figure 10. VGM temporal response; +40 to +30 V dc,  $0.4\ \mu\text{m}$  grating substrates perpendicularly disposed, 2 sec/div.



(a)



(b)



(c)

Figure 11. VGM frequency response; -40 to +20 V, 1  $\mu$ m grating substrates, 1 Hz to 30 Hz sweep. (a) Square wave; (b) Sine wave; (c) Sawtooth wave.

(c), the -40 to +30 V temporal response using square, sine and sawtooth wave excitation, respectively, swept from 1 to 30 Hz. There is clearly significant response to beyond 10 Hz. Most noteworthy is the strong spiking, mentioned earlier, which can now be seen to be most prominent at a certain intermediate range of driving frequencies, depending upon whether square, sine, or sawtooth waves are employed. It would seem possible to drive devices with these waveforms and implement the rapid response implied by these experiments.

#### B. PHYSICAL ORIGIN OF THE VARIABLE GRATING MODE EFFECT

Obviously, the important VGM device operational properties depend on the detailed nature of the grating formation and dynamic orientation process. We have, in conjunction with our colleagues at USC, made some experimental and theoretical studies this year to elucidate the fundamental nature of the grating and of the physical mechanisms that give rise to the observed periodic instability and its dynamics.

The grating produced by the periodic spatial re-orientation of the nematic liquid crystal molecules is quite unusual and gives rise to striking polarization-dependent properties in optical diffraction. By studying the intensity and polarization of the diffracted light for each diffracted order, we have been able to determine the spatial distribution of the molecular orientation within the VGM liquid crystal layer. The polarization dependence of the diffraction is due to the birefringent phase grating in which the orientation, the principal axis of the index ellipsoid, varies periodically both in the plane of the grating and normal to the plane. The spatial distribution of the ends of the liquid crystal molecules is approximately cycloidal. This was determined by matching the experimental results with theoretically calculated values for different possible models. The technical details are described in a

preliminary publication reproduced in the appendix. A more detailed publication is being prepared as well.

A theoretical study of the spatial distribution of the liquid crystal molecules is also being carried out by direct minimization of the free energy. The preliminary results of this study show that the angular dependence observed experimentally can be predicted theoretically. The origin of the VGM effect is still in doubt, but the evidence strongly points to the converse flexoelectric effect. The details of this theoretical work to date are also reproduced in the appendix.

The dynamics of grating formation, reorientation and relaxation are subjects of on-going experimental and theoretical investigation. Understanding of the basic physical principles underlying these effects is vital to the success of efforts to improve the VGM response time.

#### C. ALTERNATIVES TO THE VGM DEVICE

The variable grating mode liquid crystal effect provides only one possible means of achieving parallel intensity to position encoding. The processing potential of the intensity-to-position algorithm is so great that we have been exploring alternative implementations. One promising possibility is electro-optic beam deflection, as discussed previously. The angle that light is deflected by refraction from a prism of a small angle is approximately proportional to the prism angle and the index of refraction. The index refraction can be varied by electro-optically in many materials; the effect is particularly large in LCs where the change in index between the extremes of ordinary and extra-ordinary polarizations can be as much as 0.2 with relatively small voltages ( $\sim 10$  V). By varying the voltage locally to conform to a 2-D image which illuminates a photoconductive layer on top of a prismatic wedge of LC, one would have a device that transforms local image intensity into local angles of deflection.

In the back focal plane of a lens, these angles are mapped into displacements, i.e., a spatial Fourier transform space, with the new additional parameter of intensity included as well, just as in the VGM device. In the last period we demonstrated electro-optic deflection with liquid crystal material. The problem encountered was the very slow response time of thick liquid cells. In order to bring the response time to the millisecond region we conceived of an array of replicated little deflecting prisms. Since only the wedge angle determines the deflection of the prism and not its thickness, the array of little prisms could effect the same deflection without the disadvantages of slow speed and cloudiness caused by large thicknesses. Our past attempts to construct such structures in metal and in glass have thus far proven difficult and expensive. However, we have devised a new idea to solve the problem. We are in the process of fabricating the periodic structure by using a technique developed for other purposes at our laboratory: the anisotropic etching of silicon for the production of blazed diffraction gratings. This work was done to much finer tolerances and smaller dimensions than we require for our application.

Anisotropic etching of single crystal silicon is crystal orientation dependent. Silicon has a diamond cubic crystal structure. The anisotropic etch rate in the (100) direction is typically greater than the (110), which is greater than the (111) direction. The etching process is influenced by the crystallographic orientation of the substrate, the alignment of the grating mask pattern to the crystal orientation, and the etchant chemical.

The fabrication process basically involves a substrate with the proper crystal orientation to achieve a particular grating shape or blazed angle. A  $\text{SiO}_2$  layer is thermally grown onto the substrate to serve as a chemical mask for the anisotropic etching. Lithographic patterning of the grating is

initially done in a photoresist layer over the oxide. Alignment of the grating pattern to the crystal orientation is important to achieve proper groove shape. This pattern is transferred into the oxide coatig by acid etching or by reactive plasma etching. The substrate is then exposed to the anisotropic chemical etchant, such as potassium hydroxide (KOH).

Although symmetric grating profiles can be fabricated using this technique, well controlled blazed profiles are also achievable. For example, if a  $\text{SiO}_2$  mask is aligned along a (110) direction of a (100) silicon slice (see Figure 12), V-shaped grooves are produced with smooth (111) walls. Unlike isotropic chemical etching, the etch progresses in the (100) direction and is terminated at a depth of .707 of the oxide opening width, where the etch front meets the (111) planes, intersecting the (100) plane at the edge of the mask opening. The apex angle of the groove is  $109.47^\circ$ . To fabricate blazed structures, the silicon substrate can be cut and polished to achieve the desired blazed angle (see Figure 13). Note that apex angles of either  $109.47^\circ$  or  $70.53^\circ$  are attainable, depending upon the crystal cut. Recently, we have, on another program, fully fabricated a short period (two micrometers) grating in a single crystal silicon with significantly reduced flat top defect (Figure 14). This period is several times smaller than that which would be required for this program.

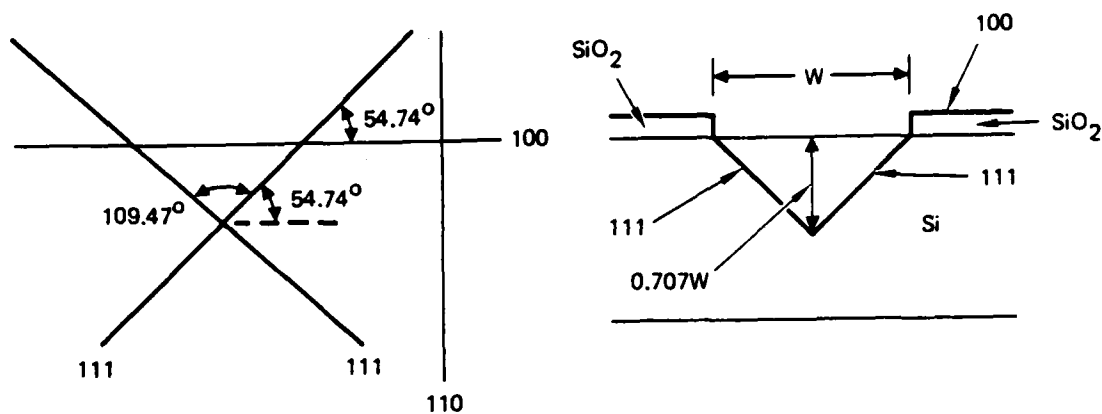


Figure 12. V-shaped grooves with (111) walls are produced by etching in (100) silicon slice.

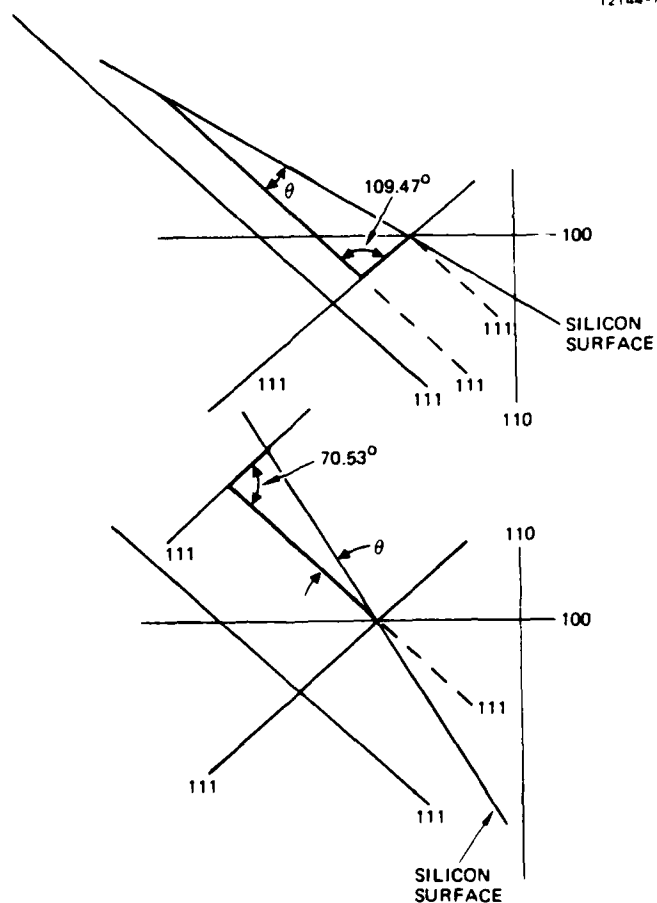


Figure 13. Blaze angle is determined by inclination angle between the silicon surface and the (111) plane.

13645-1

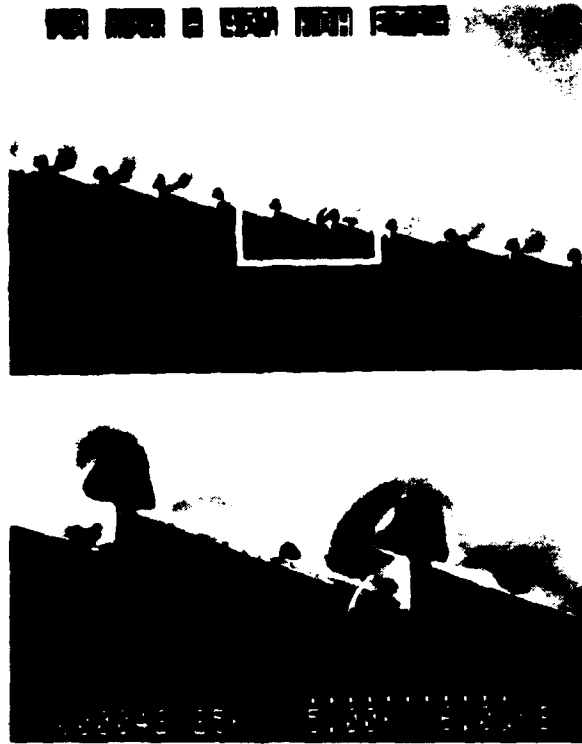


Figure 14. Short period grating in single crystal silicon.

### SECTION 3

#### PERSONNEL

The professional personnel associated with this research effort at HRL during this period were Bernard H. Soffer, principal investigator and program manager, Don Boswell, Anna Lackner, and David Margerum.

#### SECTION 4

#### PUBLICATIONS/PRESENTATIONS RESULTING FROM AFOSR SUPPORT

##### A. PUBLICATIONS

This section lists written publications for AFOSR support from the initiating date.

1. A. Armandoswell, A.A. Sawchuk, B.H. Soffer, and T.C. Strand, "Real-Time Nonlinear Optical Processing with Liquid Crystals," Proceedings 1978 International Optical Eng Conference, London, 153-158 (September 1978).
2. A. Armandoswell, A.A. Sawchuk, B.H. Soffer, and T.C. Strand, "Approaches to Nonlinear Optical Processing in Real-Time," Proceedings International Commission for Optics Congress, Spain, 253-256 (September 1978).
3. A. Armandoswell, J. Michaelson, A.A. Sawchuk, B.H. Soffer, and T.C. Strand, "Real-Time Nonlinear Processing Half-Tone Screens," 1978 Annual Meeting, Optical Society of America, San Francisco, October 1978, J. Opt. Soc. Am. 68, 1361 (October 1978).
4. A. Armandoswell, A.A. Sawchuk, G.H. Soffer, and T.C. Strand, "New Methods for Real-Time Nonlinear Optical Processing," 1978 Annual Meeting, Optical Society of America, San Francisco, California, October 1978, J. Opt. Soc. Am. 61 (October 1978).
5. A. Armandoswell, A.A. Sawchuk, T.C. Strand, D. Boswell, B.H. Soffer, "Real-Time Parallel Optical Analog-to-Digital Conversion," Optics Lett. 5, 129-131 (March 1980).
6. B.H. Soffer, D. Boswell, A.M. Lackner, A.R. Tanguay, Jr., T.C. Strand, A.A. Sawchuk, "Variable Grating Mode Liquid Crystal Device for Optical Processing," Proceedings Society of Photo-Optical Instrumentation Engineers Los Angeles Technical Symposium - Devices and Systems for Optical Signal Processing, 81-87, Los Angeles, CA, February 1980.
7. B.H. Soffer, D. Boswell, A.M. Lackner, P. Chavel, A.A. Sawchuk, T.C. Strand, and A.R. Tanguay, Jr., "Optical Computing Variable Grating Mode Liquid Crystal Devices," Proceedings Society of Photo-Optical Instrumentation Engineers Technical Symposium East - 1980, Optical Eng Conference 232, 128-136, Washington, D.C., April 1980.

8. P. Chavel, A.A. Sawchuk, T.C. Strand, A.R. Tanguay, Jr., and B.H. Soffer, "Optical Logic with Variable Grating Mode Liquid Crystals Devices," Optics Lett. 5, 398-400, September 1980.
9. B.H. Soffer, J.D. Margerum, A.M. Lackner, D. Boswell, A.A. Sawchuk, A.R. Tanguay, T.C. Strand, and P. Chavel, "Variable Grating Mode Liquid Crystal Device for Optical Processing and Computing," Molecular Crystals and Liquid Crystals 70, 145-161 (1981).
10. A.A. Sawchuk, T.C. Strand, and B.H. Soffer, "Intensity to Spatial Frequency Transformation in Optical Signal Processing, Proceeding SPIE "Advanced Inst. on Transformations in Optical Signal Processing." (February 1981).
11. A. Armand, T.C. Strand, A.A. Sawchuk, and B.H. Soffer, "Real-Time Parallel Logarithmic Filtering," Opt Lett. 7, 451-453, September 1982.
12. A.R. Tanguay, Jr., C.S. Wu, P. Chavel, T.C. Strand, A.A. Sawchuk, and B.H. Soffer, "Physical Characterization of the Variable Grating Mode Device," Opt. Eng., 22, 687-694 (1983).
13. A.R. Tanguay, Jr., P. Chavel, T.C. Strand, C.S. Wu, and B.H. Soffer "Polarization Properties of the Variable Grating Mode Liquid Crystal Device," submitted to Optics Letters.

#### B. ORAL PRESENTATIONS

This section lists oral presentations at meetings and conferences describing research supported by this contract from the initial starting date.

1. A. Armand, D. Boswell, A.A. Sawchuk, B.H. Soffer, and T.C. Strand, "Approaches to Nonlinear Optical Processing with Liquid Crystal Devices," presented at the 1978 International Optic Computing Conference, London (September 1978).
2. A. Armand, D. Boswell, A.A. Sawchuk, B.H. Soffer, and T.C. Strand, "Approaches to Nonlinear Optical Processing in Real-Time," presented at the International Commission for Optics Congress, Madrid, Spain (September 1978).

3. A. Armand, D. Boswell, J. Michaelson, A.A. Sawchuk, B.H. Soffer, and T.C. Strand, "Real-Time Nonlinear Processing with Halftone Screens," presented at 1978 Annual Meeting, Optical Society of America, San Francisco, California (October 1978).
4. A. Armand, D. Boswell, A.A. Sawchuk, B.H. Soffer, and T.C. Strand, "New Methods for Real-Time Nonlinear Processing," presented at 1978 Annual Meeting, Optical Society of America, San Francisco, California (October 1978).
5. A.A. Sawchuk, T.C. Strand, A.R. Tanguay, Jr., P. Chavel, D. Boswell, and B.H. Soffer, "Parallel Optical Analog-to-Digital Conversion Using a Liquid Crystal Light Valve," Workshop on High Speed A/D Conversion, Portland, Oregon (February 1980).
6. B.H. Soffer, D. Boswell, A.M. Lackner, A.R. Tanguay, Jr., T.C. Strand, and A.A. Sawchuk, "Variable Grating Mode Liquid Crystal Device for Optical Processing," presented at SPIE Los Angeles Technical Symposium-Devices and Systems for Optical Processing, Los Angeles, California (February 1980).
7. B.H. Soffer, D. Boswell, A.M. Lackner, P. Chavel, A.A. Sawchuk, T.C. Strand, and A.R. Tanguay, Jr., SPIE Technical Symposium East - 1980 Optical Computing Conference, Washington, D.C. (April 1980).
8. A.A. Sawchuk, T.C. Strand, A.R. Tanguay, Jr., P. Chavel, D. Boswell, A.M. Lackner, and B.H. Soffer, "Variable Grating Model Liquid Crystal Light Valves and Their Application to Optical Processing," Gordon Research Conference on Coherent Optics and Holography, Santa Barbara, California (June 1980).
9. B.H. Soffer, D. Boswell, A.M. Lackner, A.R. Tanguay, Jr., T.C. Strand, and A.A. Sawchuk, "Variable Grating Mode Liquid Crystal Devices for Optical Processing and Computing," Eighth International liquid Crystal Conf., Kyoto, Japan (June 1980).
10. A.R. Tanguay, Jr., T.C. Strand, P. Chavel, B.H. Soffer, and A.S. Sawchuk, "Theoretical and Experimental Polarization Properties of the Variable Grating Mode Liquid Crystal Structure," presented at Annual Meeting of Optical Society of America, Orlando, FL, Oct. 1981.

11. B. H. Soffer, "Technical Applications of the Variable Grating Mode Effect," presented at 4th Liquid Crystal Conference, Tbilisi, Georgia, USSR, Sept. 1981.
12. B.K. Jenkins, A.A. Sawchuk, B.H. Soffer, and T.C. Strand, "Sequential Optical Logic Implementation," presented at Annual Meeting of Optical Society of America, Tucson, AZ Oct. 1982.
13. U. Efron, B.H. Soffer, M.J. Little, and H.J. Caufield, "The Application of Silicon Liquid Crystal Light Valves to Optical Data Processing," presented at the SPIE Technical Symposium - Advances in Optical Information Processing, (V. 388) LA, January 1983.
14. A.R. Tanguay, Jr., C.S. Wu, P. Chavel, T.C. Strand, A.A. Sawchuk, and B.H. Soffer, "Physical Characterization of the Variable Grating Mode Liquid Crystal Device," presented at the SPIE Technical Symposium - Advanced Optical Information Processing (V. 388) LA, January 1983.
15. U. Efron, B.H. Soffer, and H.J. Caufield, "The Application of Silicon Liquid Crystal Light Valves to Optical Data Processing: A Review," presented at Optical Information Processing Conference II, NASA, Langley, VA Aug. 1983.
16. B.H. Soffer, "Liquid Crystal Optical Processing," invited keynote paper presented at 13th European Solid State Device Research Conference, University of Kent at Canterbury, Sept. 1983.

APPENDIX

PHYSICAL CHARACTERIZATION OF THE VARIABLE GRATING MODE  
LIQUID CRYSTAL DEVICE

# Physical characterization of the variable grating mode liquid crystal device

A. R. Tanguay, Jr.  
C. S. Wu  
P. Chavel\*  
T. C. Strand†  
A. A. Sawchuk

University of Southern California  
Image Processing Institute, and Departments of  
Electrical Engineering and Materials Science  
Los Angeles, California 90089-0483

B. H. Soffer

Hughes Research Laboratories  
3011 Malibu Canyon Road  
Malibu, California 90265

**Abstract.** The physical principles of operation of the variable grating mode (VGM) liquid crystal device are described. The VGM device is capable of performing a two-dimensional intensity-to-spatial frequency conversion, which in turn allows the implementation of a wide range of nonlinear optical processing and computing functions. The device utilizes certain nematic liquid crystal mixtures that are observed to form variable frequency diffraction gratings under the influence of an applied bias voltage. Both fundamental and technological limitations to device performance characteristics are discussed.

**Keywords:** spatial light modulator; variable grating mode; liquid crystal device; optical information processing; optical devices.

*Optical Engineering* 22(6), 687-694 (November/December 1983).

## CONTENTS

1. Introduction
2. Device description and operational mode
3. Fundamental origins of the operational properties
4. Physical origin of the variable grating mode effect
5. Acknowledgments
6. References

## 1. INTRODUCTION

A wide variety of one- and two-dimensional operations are necessary for full-scale implementation of parallel optical processing and computing systems. Incoherent-to-coherent conversions are often required for algorithms involving spectrum analysis and modification, correlation, convolution, and holographic image formation, particularly when the information to be processed is available only in time-sequential or matrix-addressed raster format. A number of one- and two-dimensional spatial light modulators capable of this type of image transduction are described within this special issue of *Optical Engineering*,<sup>1-4</sup> as well as in several review articles.<sup>5-8</sup>

Other, equally important processing and computing functions, such as logic operations, programmable matrix addressing, binary addition, linearity compensation, and input-output nonlinearities (e.g., exponentials, logarithms, power laws, thresholds, level slices, and level restoration), have proven particularly difficult to implement. All of these functions, on the other hand, can be implemented by means of some form of intensity-to-position encoding in conjunction with either fixed (single function) or programmable (multifunction) masks. This general statement follows from the realization that all of the functions listed above are special cases of data-dependent multiplications, in which the input value (e.g., pixel intensity) selects the appropriate multiplier (e.g., mask location) to obtain the desired product (e.g., output intensity).

\* Permanent address: Institut d'Optique, Université de Paris sud, BP 43, 91406 Orsay Cedex, France

† Present address: IBM Corporation, 5600 Cottle Rd., San Jose, CA 95193.

Invited Paper L.M.-104 received July 15, 1983; revised manuscript received July 28, 1983; accepted for publication Aug. 7, 1983; received by Managing Editor Aug. 29, 1983. This paper is a revision of Paper 388-12 which was presented at the SPIE conference on Advances in Optical Information Processing, Jan. 20-21, 1983, Los Angeles, CA. The paper presented there appears (unrefereed) in SPIE Proceedings Vol. 388.  
© 1983 Society of Photo-Optical Instrumentation Engineers.

The variable grating mode liquid crystal device (VGM LCD)<sup>9-12</sup> transforms input intensities to spatial positions when used in conjunction with a Fourier transform lens. The nature of this image transformation can be realized in the following manner. The VGM LCD primarily consists of a photoconductive layer in series with a layer of nematic liquid crystal mixture. A dc bias voltage is applied across the device to provide a voltage division between the two layers. Within a given image pixel, the input intensity decays the voltage across the photoconductive layer and correspondingly enhances the voltage across the liquid crystal layer. The photoconductor thus implements an intensity-to-voltage conversion. The nematic liquid crystal mixture employed in the device has the unusual property that the alignment of the liquid crystal molecules, which is homogeneous in the quiescent state, exhibits spatially periodic modulation when a bias voltage is applied across the layer. This modulation results in a birefringent phase grating<sup>13</sup> characterized by a spatial frequency that depends linearly on the applied voltage. The effect of the liquid crystal layer is thus to implement a voltage-to-spatial frequency conversion. If both layers are considered together, the entire device is thus seen to perform an image-wise intensity-to-spatial frequency conversion, which can be modified to the more general intensity-to-position transformation by placing a Fourier transform lens behind the VGM LCD. Collimated readout illumination normally incident on the device (at a wavelength of photoconductive insensitivity) is angle encoded within each image pixel by diffraction from each induced phase grating and subsequently angle-to-position mapped by the Fourier transform lens into its focal plane.

This type of process is shown schematically in Fig. 1, in which the input image is assumed to consist of two separate regions of differing intensity. The VGM LCD encodes both regions with different spatial frequencies, resulting in separated diffraction orders in the filter (Fourier) plane. Insertion of an appropriate spatial filter or programmable mask (not shown in Fig. 1) into the Fourier plane allows the separated orders to be selectively modified to implement any desired data-dependent multiplication or point nonlinearity. In the reconstructed output image, all regions of equal input intensity are modified identically, irrespective of their location in the input image field. Thus, all of the data-dependent multiplications are performed in parallel. Functional programmability is achieved by replacement or reprogramming of the Fourier plane mask, which need only be a low resolution device with a total number of resolution elements equal to the number of gray levels required to be processed.

The overall input-output characteristic of nonlinear function

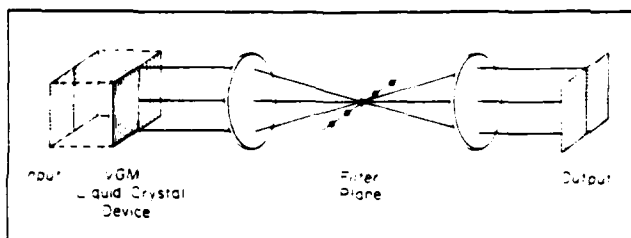


Fig. 1. Experimental arrangement for demonstration of intensity-to-position encoding by means of an intensity-to-spatial frequency conversion in a VGM LCD.

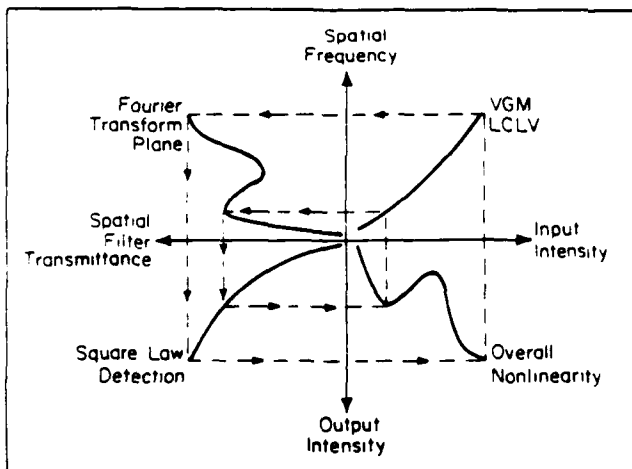


Fig. 2. VGM nonlinear processing. The overall input-output characteristic can be found by stepping through the successive nonlinear transformations, including (1) the intensity-to-spatial frequency conversion, (2) spatial filtering, and (3) intensity detection.

implementation utilizing the VGM LCD is shown schematically in Fig. 2 by specifying sequentially the nature of the transformations from input intensity to spatial frequency within the VGM LCD, from spatial frequency to spatial filter amplitude transmittance in the Fourier transform plane, and from output amplitude to output intensity (usually by means of square law detection). The overall nonlinearity achieved can be easily compensated for the functional dependences of the separate steps by adjustment of the selected spatial filter transmittance function.

The VGM LCD has thus far been utilized to perform a wide variety of parallel nonlinear point transformations, including level slicing,<sup>9,10,12</sup> binary logic functions (AND, OR, NOR, etc.),<sup>10-12</sup> and full binary addition (inputs: two addend bit planes and one carry bit plane; outputs: sum bit plane and carry bit plane).<sup>11</sup> The purpose of this paper is to describe the physical principles of operation of the variable grating mode liquid crystal device, identify areas of strength and weakness, and differentiate limitations to current device performance thought to be fundamental in origin from those that are seemingly technological. Section 2 consists of a more detailed description of the device, its operating mode, and its operational properties. The fundamental origins of these operational properties are examined in Sec. 3, in which the natural focus will be the physical mechanism of the variable grating mode effect in nematic liquid crystal mixtures. Experimental and theoretical efforts to elucidate the nature of this mechanism are described in Sec. 4, which concludes with several important but as yet unanswered questions.

## 2. DEVICE DESCRIPTION AND OPERATIONAL MODE

A number of important aspects of device construction and device operation are reviewed in this section. A more complete description

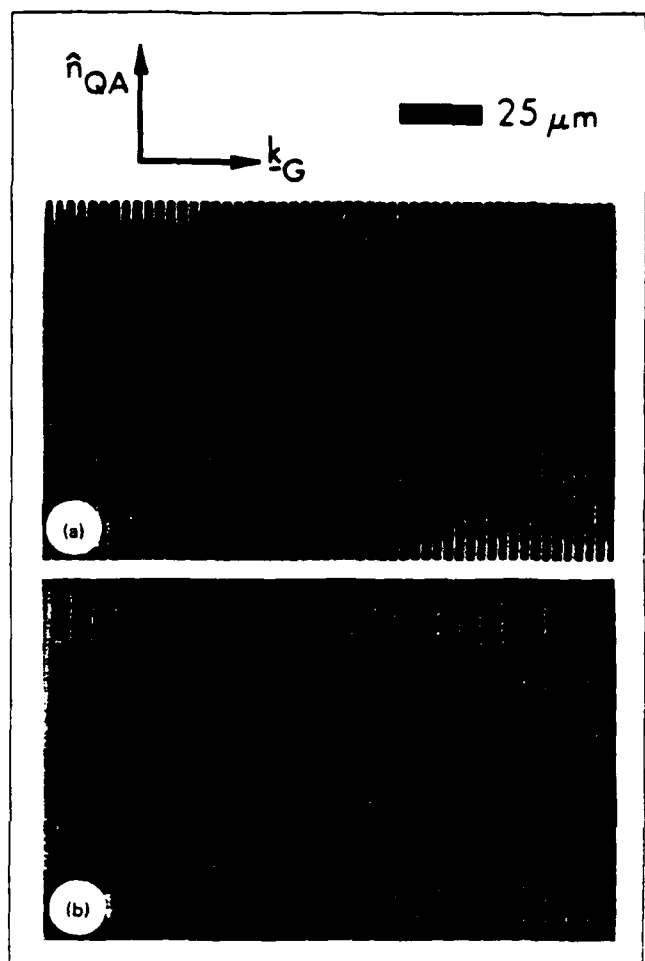


Fig. 3. Polarization photomicrographs of the liquid crystal domain pattern in an electrically activated cell. In (a), the polarizer was oriented at  $90^\circ$ , and the analyzer at  $90^\circ$ , with respect to the grating wave vector. In (b), the polarizer was oriented at  $90^\circ$ , and the analyzer at  $10^\circ$ , with respect to the grating wave vector. The unit vector  $\hat{n}_{QA}$  denotes the direction of quiescent alignment, and  $k_G$  indicates the direction of the grating wave vector.

of these concepts has appeared previously.<sup>9-12</sup>

The critical element of the VGM LCD is a thin (4 to  $12 \mu m$ ) layer of nematic liquid crystal mixture<sup>12</sup> that exhibits a periodic modulation of the liquid crystal director, and hence of the index ellipsoid, under application of an electric field normal to the plane of the layer. By means of suitable preferential alignment techniques,<sup>9,12</sup> the quiescent state of the liquid crystal is homogeneous (parallel to the plane of the layer). As will be discussed in Sec. 4, this periodic variation of the principal axes of the dielectric tensor gives rise to a birefringent phase grating characterized by striking and unique optical properties.<sup>14</sup> The grating can be visualized in a polarizing microscope, as shown in Fig. 3, by utilizing the birefringence properties of the periodic perturbation. Distinct polarizer analyzer combinations give rise to remarkably different grating images, as can be seen by comparison of Figs. 3(a) and 3(b) (see Sec. 4). Furthermore, the grating period is observed experimentally to be related inversely to the applied voltage across the layer. Above the threshold for domain formation, therefore, the spatial frequency of the grating is a linear function of the voltage across the layer, as shown for a variety of nematic liquid crystal mixtures in Fig. 4.

This voltage-to-spatial frequency transformation can be optically

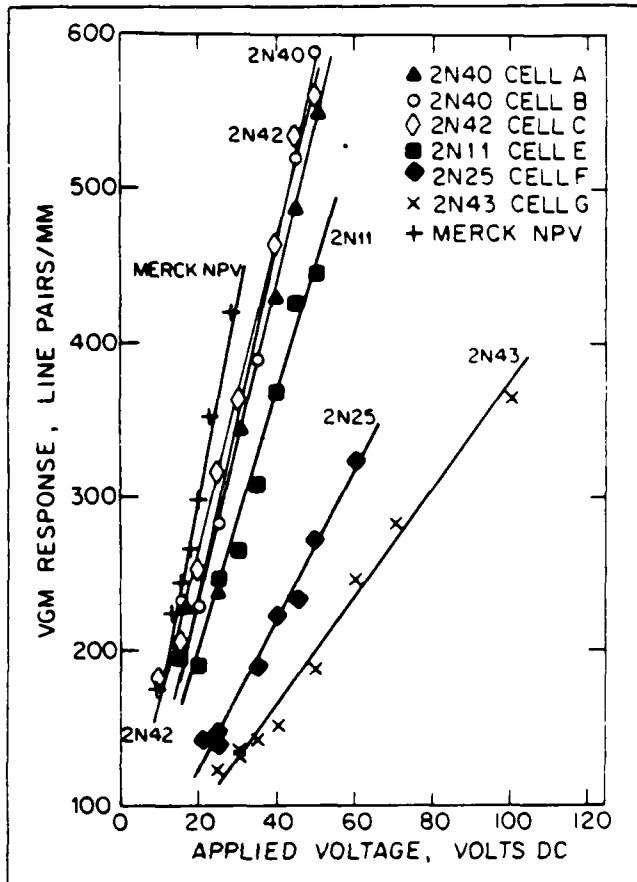


Fig. 4. VGM spatial frequency as a function of applied voltage for various nematic liquid crystal mixtures.

addressed by means of a photoconductor placed in series with the liquid crystal layer, as shown in Fig. 5 and described in the previous section. The photoconductive layer employed in devices constructed thus far is comprised of evaporated or ion-beam sputtered zinc sulfide (ZnS), chosen to optimize the impedance match with the liquid crystal layer ( $\rho > 10^{10} \Omega \cdot \text{cm}$ ). The layer thicknesses employed were of order 1.5 to 5  $\mu\text{m}$ . As shown in Fig. 5, the photoconductive and liquid crystal layers are sandwiched between indium tin oxide (ITO)-coated 1.2 cm thick glass optical flats. The liquid crystal layer thickness is determined by a perimeter Mylar spacer.

In operation, a dc bias voltage is applied between the indium tin oxide electrodes, of order 40 to 150 V. The input image to be spatial frequency encoded is focused on the ZnS photoconductor, producing image-wise modulation of the local voltage across the liquid crystal layer, thus effecting a parallel intensity-to-spatial frequency conversion. The high lateral impedance of the thin film layers allows high resolution images to be processed with low pixel-to-pixel crosstalk. The device sensitivity is optimized for exposure at blue and near-ultraviolet wavelengths due to the peak photosensitivity of zinc sulfide in that spectral region. Quasi-nondestructive readout can be accomplished at wavelengths beyond the photoconductivity edge, such as that of the He-Ne laser (6328 Å). Image erasure occurs with removal of the input image, within the dielectric and liquid crystal relaxation times of the device (see Sec. 3). To date, all VGM LCDs that we have constructed have been designed for transmissive readout, although reflective readout is possible with incorporation of an appropriate dielectric mirror. Such a configuration would have the advantage of fully separating the reading and writing functions, allowing for increased effective optical gain.

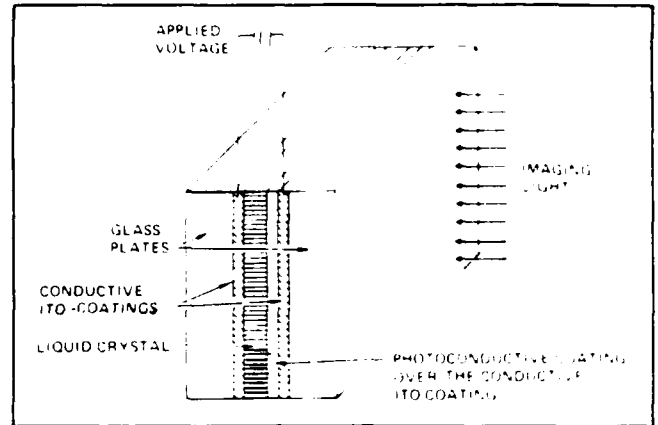


Fig. 5. Schematic diagram of the VGM liquid crystal device. Current devices are read out in transmission at a wavelength of photoconductive insensitivity.

### 3. FUNDAMENTAL ORIGINS OF THE OPERATIONAL PROPERTIES

As was mentioned in Sec. 2, the operational properties of the VGM LCD are primarily determined by the variable grating mode effect exhibited by the nematic mixture liquid crystal layer. The current state of knowledge concerning the physical origin of this unique effect is summarized in Sec. 4. In this section, we outline a number of key factors and considerations that affect several important device properties in order to provide both focus and a frame of reference for the succeeding section. These device properties include the accessible range of spatial frequencies, the number of accessible gray levels, the functional dependence of diffraction efficiency on applied voltage, maximum diffraction efficiency, response time, device uniformity, device input sensitivity, and device operational lifetime.

The accessible range of spatial frequencies extends from the threshold for grating formation at the low end to the onset of dynamic scattering induced by high electric fields at the high end, as shown in Fig. 4. For phenyl benzoate mixtures with slightly negative dielectric anisotropy ( $< -0.30$ ) such as HRL 2N40,<sup>15</sup> this range extends from approximately 200 line pairs/mm to over 600 line pairs/mm. In order to avoid overlap of higher diffracted orders from lower spatial frequencies with lower diffracted orders from higher spatial frequencies, the maximum range that can be processed (uniquely assigned to specific gray levels) spans a factor of two in spatial frequency. For example, a usable range in HRL 2N40 extends from 300 line pairs/mm to 600 line pairs/mm without order overlap. This accessible range can be extended by an additional factor of two by utilizing the orthogonal polarization behavior of alternating diffracted orders, as described in Sec. 4. Hence, the accessible range of spatial frequencies observed in several of the nematic liquid crystal mixtures tested so far is sufficient for optimized gray scale processing. It should be noted that although the maximum number of resolution elements that can be processed is linearly proportional to the highest spatial frequency utilized for devices of a given size (see discussion below), use of significantly larger spatial frequencies begins to place stringent requirements on the Fourier transform lens due to f-number reduction. For example, to utilize a spatial frequency range of 600 line pairs/mm requires the output optics to have an f-number less than 1.2 (or less than 2.6 if the lens is displaced off-axis to accept only the positive diffracted orders). This is primarily a pragmatic limitation rather than a fundamental one, as VGM effects have been observed at spatial frequencies exceeding 1000 line pairs/mm.<sup>16</sup>

The number of accessible gray levels that lead to well-separated diffraction orders in the filter plane is limited by the ratio of the frequency range between VGM harmonics to the object spectrum bandwidth, as shown in Fig. 6. The object spectrum bandwidth is in turn limited primarily by two effects: spot size due to diffraction from

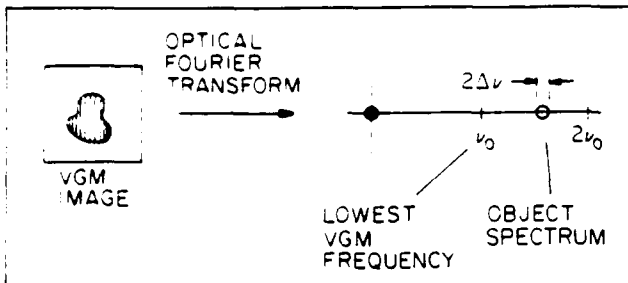


Fig. 6. Gray level resolution. The number of accessible gray levels is limited by the ratio of the separation between VGM harmonics to the object spectrum bandwidth.

finite-sized pixel apertures, and grating imperfections that cause local deviations from uniform spatial frequency. The first effect is fundamental and has been treated previously.<sup>10</sup> The principal result of this analysis is the inequality

$$b\nu_0 \geq 2N \quad (1)$$

in which  $b$  is the pixel width,  $\nu_0$  is the lowest usable VGM spatial frequency, and  $N$  is the desired number of distinguishable gray levels. This inequality requires that the pixel size contain at least  $2N$  periods of the lowest grating frequency if  $N$  gray levels are to be processed. For example, a  $256 \times 256$  pixel image could be processed with 32 distinguishable gray levels on a 50 mm square device with  $\nu_0 \approx 300$  line pairs/mm. An additional restriction arises from scattering effects due to grating imperfections, which tend to further increase the size of the diffracted orders. The most common type of imperfection observed in these devices is the joining or splitting of grating lines, as shown in the photomicrograph in Fig. 7. The origin of these "disclinations" is not at present understood, although the density of occurrence of such imperfections is directly related to the quality of substrate preparation.

A typical measurement of the functional dependence of diffraction efficiency on the applied voltage across the VGM liquid crystal layer is shown in Fig. 8. Since the applied voltage is linearly related to the induced grating spatial frequency, this relationship is illustrative of the dependence of the diffraction efficiency on spatial frequency as well. To first order, the nature of this dependence is not important to the implementation of optical processing functions since any variation in diffraction efficiency with spatial frequency can be linearized by insertion of an appropriate multiplicative filter in the focal plane of the Fourier transform lens. In any case, the theoretical functional dependence can be derived only from knowledge of the relationship between the induced orientational angles of the liquid crystal director and the applied voltage across the layer. This relationship is discussed further in the subsequent section.

The maximum diffraction efficiency that can be achieved at a given spatial frequency and applied voltage depends fundamentally on the magnitude of the anisotropy in the index of refraction ( $\Delta n = n_e - n_o$ , with  $n_e$  the extraordinary refractive index for polarization parallel to the molecular axis and  $n_o$  the ordinary refractive index for polarization perpendicular to the molecular axis), the magnitude of the periodic angular reorientation of the liquid crystal director, and the thickness of the VGM liquid crystal layer. Full periodic reorientation of the index ellipsoid from homogeneous (parallel to the substrate) alignment to homeotropic (perpendicular) alignment for HRL 2N40 ( $\Delta n = 0.15$ ) in a  $6 \mu\text{m}$  cell read out at  $6328 \text{ \AA}$  gives rise to an optical phase modulation of approximately 9 rad. Hence, the maximum diffraction efficiency is fundamentally limited to that expected for a pure sinusoidal phase grating.<sup>17</sup> In practice, full reorientation is typically not achieved before the onset of dynamic scattering, although reorientation angles of  $45^\circ$  are thought at present to be commonly reached (see Sec. 4). As can be seen from Fig. 8, typical second-order diffraction efficiencies are of order 20%. This

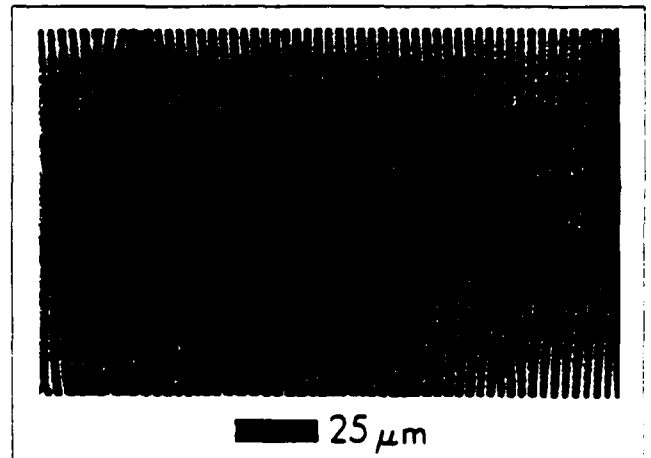


Fig. 7. Polarization photomicrograph of a VGM liquid crystal layer exhibiting a number of grating discontinuities (circled).

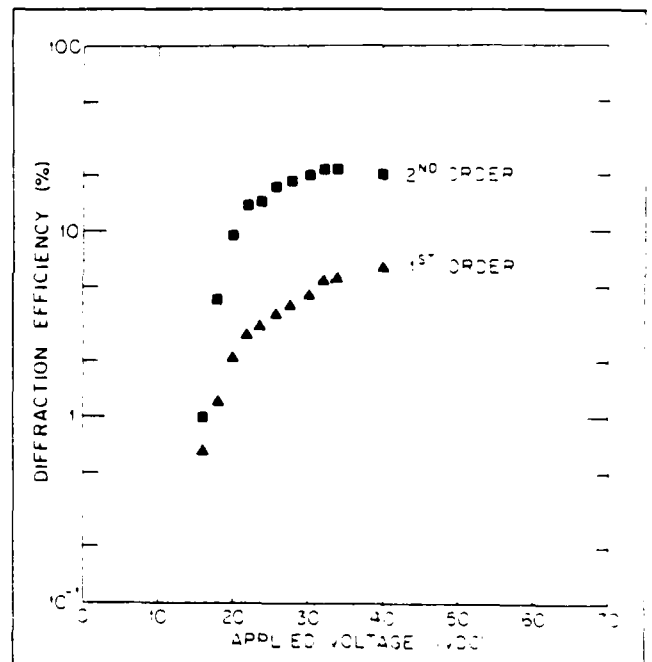


Fig. 8. Diffraction efficiency as a function of applied voltage across a nematic liquid crystal mixture of phenyl benzoates (HRL 2N40). The layer thickness was approximately  $6 \mu\text{m}$ , as defined by a perimeter Mylar spacer.

order is larger than the first diffracted order due to the peculiar nature of the birefringent phase grating formed by the VGM distortion (details are given for this phenomenon in Sec. 4).

The response time of the cell is a critical parameter that directly affects the achievable overall processing throughput rate. At present it is the major factor inhibiting widespread incorporation of VGM devices in optical processing systems. The rise time for grating formation from below to above threshold varies from mixture to mixture, but is typically of order one second. The response time for grating change in response to a step increase in applied voltage (corresponding to a step increase in grating spatial frequency) is typically of order a fraction of a second.<sup>18</sup> The response time of the photoconductive voltage division across the liquid crystal layer is not a significant factor by orders of magnitude relative to the reorien-

tation response time, so that eventual improvements in VGM LCD response time will accrue only by advances in the state of understanding of the physical origin of the VGM effect and the dynamical nature of the grating reorientation process, followed by appropriate modification of the device operational mode to enhance the rate of molecular reorientation and/or a search for a nematic liquid crystal mixture with physical characteristics optimized for dynamic VGM effects.

The input sensitivity of the VGM LCD, defined as the input (writing) intensity per unit area per unit change in grating spatial frequency, is determined by a number of factors. These include the slope of induced grating spatial frequency as a function of applied voltage for the particular nematic liquid crystal mixture employed, the wavelength dependence of the photoconductive layer photosensitivity, and the cell switching ratio (fractional increase in voltage across the liquid crystal layer from illumination at the threshold for grating formation to saturation). The first factor (liquid crystal response slope) varies significantly from mixture to mixture (see Fig. 4). Of the VGM nematic liquid crystal mixtures investigated to date, HRL 2N40 has proved to be nearly optimum in this regard. It is not yet clear what fundamentally influences and eventually limits this parameter. The photosensitivity of the photoconductive layer is determined primarily by the choice of photoconductive material (limited to those that can be appropriately impedance-matched to the liquid crystal layer), method and quality of thin film deposition, layer thickness, spectral width and central wavelength of the exposure (writing) illumination, and the operational bias voltage employed. The cell switching ratio is a function of the series impedance of the liquid crystal layer, the impedance of the unilluminated photoconductive layer, and the impedance of the photoconductive layer under saturation illumination. In addition, the cell switching ratio will be altered by incorporation of surfactant layers to improve liquid crystal quiescent alignment, and of a dielectric mirror in the reflective readout device structure. At this stage of the device development, the input sensitivity of the VGM LCD has not been optimized. A typical value of  $15 (\mu\text{W}/\text{cm}^2) \cdot (\text{mm}/\text{line pair})$  was obtained with a VGM LCD consisting of a  $6 \mu\text{m}$  layer of HRL 2N40 in series with a  $5 \mu\text{m}$  thick evaporated ZnS layer that had been polished and rubbed with surfactant polyvinyl alcohol, operated at 160 V dc, and illuminated in the passband 410 to 550 nm.<sup>9</sup>

The uniformity of VGM LCD response depends inherently on technological issues, including uniformity of layer thicknesses, homogeneous mixing of the liquid crystal material employed, and the as-deposited spatial dependence of photoconductive sensitivity. Whereas it is relatively straightforward to construct electrically activated VGM cells (see Sec. 4) that exhibit a high degree of spatial uniformity, deposition of a photoconductive layer with equivalent spatial homogeneity has proven more difficult. Nonuniformity of the device response characteristic can be a contributing factor in the establishment of the maximum number of accessible gray levels discussed previously. In experimental devices constructed thus far, device uniformity has not proven to be the limiting factor. In any case, it is expected that response nonuniformities can be minimized significantly by improvements in the photoconductive layer deposition process.

The lifetimes of experimentally constructed VGM LCDs have ranged from less than a week to over a year. The causes of VGM device failure have not yet been extensively studied, although several contributing factors can be identified. These factors include the purity and composition of the liquid crystal mixture employed, the nature of the liquid crystal/photoconductive layer interface, the integrity of the device sealing process, and the device operational history. Since the VGM effect requires a dc applied voltage, unidirectional ion poisoning may contribute to gradual device degradation.

#### 4. PHYSICAL ORIGIN OF THE VARIABLE GRATING MODE EFFECT

As can be clearly understood from the discussion presented in Sec. 3, a vast majority of the important device operational properties depend critically on the detailed nature of the grating formation and dynamic

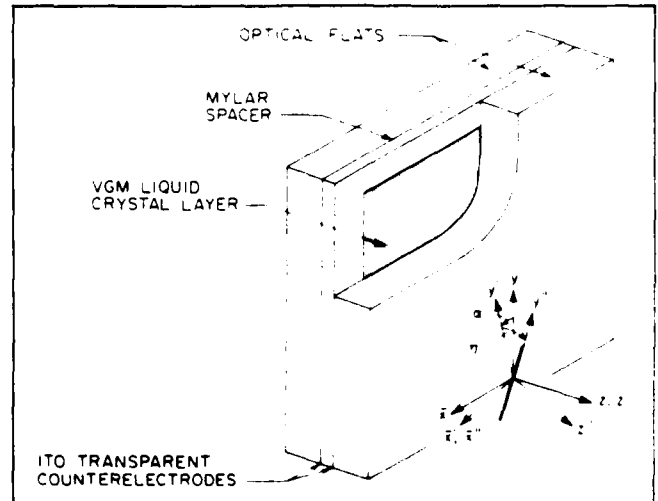


Fig. 9. Variable grating mode liquid crystal test geometry showing the Cartesian coordinate system referred to in the text as well as the molecular orientation angles  $\alpha$  and  $n$ . This configuration was utilized in the polarized light diffraction efficiency and photomicroscopy experiments.

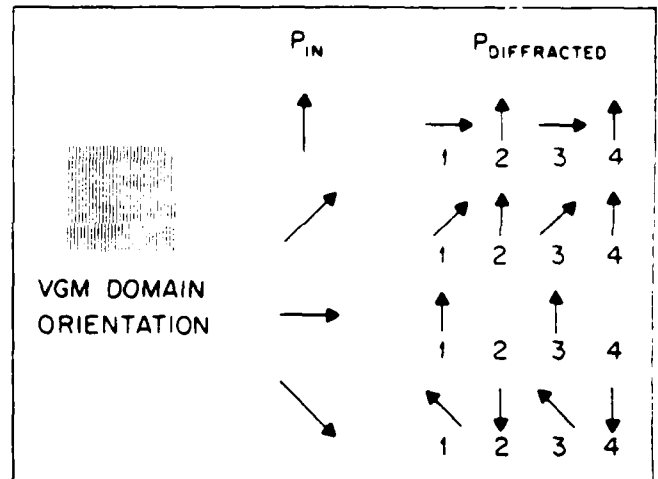


Fig. 10. The polarization behavior of VGM diffracted orders, with illumination normal to the plane of the liquid crystal layer. The left-hand column indicates the input polarization associated with each row of output polarizations. The inset shows the corresponding orientation of the VGM grating.

reorientation process. The elucidation of the fundamental nature of the grating (molecular orientation angles as a function of applied voltage across the liquid crystal layer) and of the physical mechanism that gives rise to the observed periodic instability and its reorientation dynamics has been a subject of considerable experimental and theoretical interest.<sup>11,16,19-30</sup> In this section, the present state of understanding of the VGM effect is described, and a number of important unresolved questions are presented.

The grating produced by the periodic spatial reorientation of the nematic liquid crystal molecules is quite unusual, giving rise to striking polarization-dependent properties.<sup>11</sup> These diffraction effects can be investigated in an electrically activated VGM cell with no intervening photoconductive layer, as shown in Fig. 9. The orientation of the grating is such that the grating wave vector is perpendicular to the direction of unperturbed alignment, which is homogeneous and induced by unidirectional rubbing or ion-beam milling. That is, the periodic modulation direction is perpendicular to the initial (zero applied bias) liquid crystal director (long molecular axis), as shown

in the polarization micrographs (Fig. 3).

For all linear input polarization angles, the even and odd diffraction orders are found to be essentially linearly polarized. In addition, the even diffraction orders are nearly linearly polarized parallel to the "domains" comprising the VGM grating, as shown in Fig. 10. For input polarization perpendicular to the domains, the even orders are found to be almost fully extinguished. On the other hand, the odd diffraction orders are nearly linearly polarized with a major axis that rotates counterclockwise at the same rate as the input polarization is rotated clockwise. This effect is the same as that produced by a half-wave plate oriented at  $45^\circ$  with respect to the grating wave vector. For input polarization at  $45^\circ$  to the wave vector, all orders are observed in the far-field diffraction pattern. An analyzer placed on the output side of the VGM device can be rotated to extinguish the even orders (when oriented parallel to the grating wave vector) or the odd orders (when oriented at  $-45^\circ$  to the grating wave vector).

These unusual polarization properties have recently been utilized to determine the spatial distribution of the molecular orientation within the VGM liquid crystal layer.<sup>11</sup> The polarization dependence of the diffraction phenomena is directly related to the formation of a birefringent phase grating,<sup>12</sup> in which the principal axis of the index ellipsoid varies periodically both in the plane of the grating (characterized by an orientation angle  $\alpha$ ) and normal to the plane of the grating (characterized by an orientation angle  $\eta$ ). The angular coordinates are as shown in Fig. 9.

The polarization properties of light diffracted by the liquid crystal birefringent phase grating can be summarized by means of a transfer matrix that connects the output polarization at each point  $(x, y)$  on the rear surface of the liquid crystal layer with the input polarization at the front surface of the liquid crystal layer. On the basis of the experimental observations, this matrix must be of the form

$$\begin{bmatrix} A_0 + A(x;p) & B(x;2p) \\ C(x;2p) & D_0 + D(x;p) \end{bmatrix} \quad (2)$$

in which the notation  $A(x;p)$  indicates that the complex amplitude  $A$  varies in the  $x$  direction with periodic repetition distance  $p$ . For uniaxial liquid crystal molecules at an arbitrary orientation  $(\alpha, \eta)$ , assumed uniform throughout the layer thickness at a given coordinate in the  $x$  direction, the Jones matrix can be determined by appropriate rotations of the index ellipsoid, which yields

$$\begin{bmatrix} 1 - \sin^2 \alpha (1 - e^{i\phi}) & \sin \alpha \cos \alpha (1 - e^{i\phi}) \\ \sin \alpha \cos \alpha (1 - e^{i\phi}) & 1 - \cos^2 \alpha (1 - e^{i\phi}) \end{bmatrix} \quad (3)$$

where

$$\phi = \frac{2\pi t}{\lambda} \left[ \left( \frac{\sin^2 \eta}{n_o^2} + \frac{\cos^2 \eta}{n_e^2} \right)^{-1/2} - n_o \right]$$

in which  $t$  is the liquid crystal layer thickness,  $n_o$  is the ordinary index of refraction,  $n_e$  is the extraordinary index of refraction, and  $\lambda$  is the wavelength of readout illumination employed. The angles  $\alpha$  and  $\eta$  are assumed to be periodic functions of  $x$  and independent of  $y$  and  $z$ . Measurement of the intensities in each diffraction order for a minimum set of polarizer-analyzer orientations uniquely determines the magnitudes of the Fourier components of the polarization transfer matrix. These experimentally derived values can then be compared with the theoretically calculated coefficients of Eq. (3) (by harmonic expansion) for different possible assumptions concerning the spatial distribution of the orientation angles  $\alpha$  and  $\eta$ . An example of such a comparison between theory and experiment is shown in Fig. 11, under the assumption that the spatial dependences of  $\alpha$  and  $\eta$  are given by

$$\alpha = \alpha_0 \cos \frac{2\pi x}{\Lambda} \quad (4)$$

$$\eta = \pm \eta_0 \sin \frac{2\pi x}{\Lambda}$$

This procedure allows the extraction of the maximum orientational excursion angles  $\alpha_0(V)$  and  $\eta_0(V)$  as functions of the applied bias voltage above the threshold for grating formation, as shown in Fig. 12 ( $\alpha_0$ ) and Fig. 13 ( $\eta_0$ ). In each case, subject to the assumed forms of  $\alpha$  and  $\eta$  implicit in Eq. (4), it is observed that the maximum excursion angles both in and out of the plane of the grating seem to increase as the logarithm of the applied voltage.

The spatial distribution of the ends of the liquid crystal molecules described by Eq. (4) is approximately cycloidal. Such a dependence of the angles  $\alpha$  and  $\eta$  on the spatial coordinate  $x$  has been predicted by direct minimization of the free energy in a similar nematic liquid crystal system.<sup>21</sup> This particular solution is obtained by incorporation of the converse flexoelectric effect in the expression for the free energy.<sup>13, 21-23</sup> The flexoelectric effect describes a strain-induced polarization that arises due to molecular shape effects in conjunction with a nonzero dipole moment, as shown schematically in Fig. 14. The converse flexoelectric effect thus pertains to a polarization-induced strain within the liquid crystal layer, which can result in a periodic molecular reorientation characterized by a linear dispersion relation between the grating wave vector and the applied field, as is observed experimentally. Including the dielectric, distortion, and flexoelectric contributions to the free energy, yields an expression of the form

$$\begin{aligned} F_{VGM} &= \int (F_{\text{dielectric}} + F_{\text{distortion}} + F_{\text{flexoelectric}}) dV \\ &= F_0 - \frac{1}{8\pi} \int (\epsilon_e - \epsilon_o) (\mathbf{E} \cdot \hat{n})^2 dV \\ &\quad + \frac{1}{2} \int [K_1 (\nabla \cdot \hat{n})^2 + K_2 (\hat{n} \cdot \nabla \times \hat{n})^2 \\ &\quad + K_3 (\hat{n} \times \nabla \times \hat{n})^2] dV \\ &\quad - \int [e_1 (\nabla \cdot \hat{n}) (\hat{n} \cdot \mathbf{E}) \\ &\quad + e_3 \{ (\nabla \times \hat{n}) \times \hat{n} \} \cdot \mathbf{E}] dV \end{aligned} \quad (5)$$

in which  $K_1$ ,  $K_2$ , and  $K_3$  are the elastic constants for splay, twist, and bend deformations, respectively;  $\hat{n}$  is the liquid crystal director;  $\mathbf{E}$  is the applied electric field;  $\epsilon_e$  and  $\epsilon_o$  are principal components of the dielectric tensor of the liquid crystal; and  $e_1$  and  $e_3$  are flexoelectric coefficients.<sup>21</sup> Minimization of  $F_{VGM}$  with respect to the orientation angles  $\alpha$  and  $\eta$  of the director, subject to fully pinned boundary conditions at both substrate surfaces, and with the simplifying assumption that  $K_1 = K_2 = K$ , yields<sup>21</sup>

$$\begin{aligned} \alpha &= \alpha_0 \cos(kx) \cos(\pi z/t) \\ \eta &= \eta_0 \sin(kx) \cos(\pi z/t) \end{aligned} \quad (6)$$

in which  $k$  is the grating wave vector, and  $t$  is the liquid crystal layer thickness. This solution generates a dispersion relation between  $E$  and  $k$  of the form

$$E^2 = \left( \frac{K}{\epsilon_o} \right)^2 \cdot \frac{[k^2 + (\pi/t)^2]^2}{k^2 + \mu[k^2 + (\pi/t)^2]} \quad (7)$$

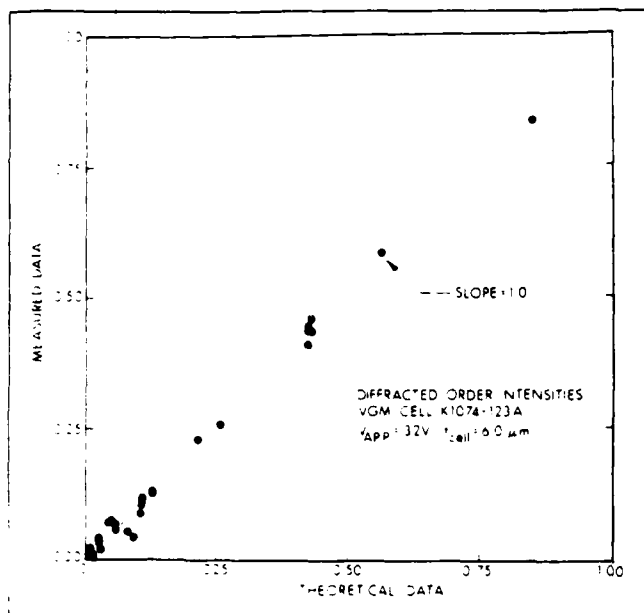


Fig. 11. Measured diffracted order intensities as a function of theoretical intensities calculated from the uniaxial VGM model described in the text.

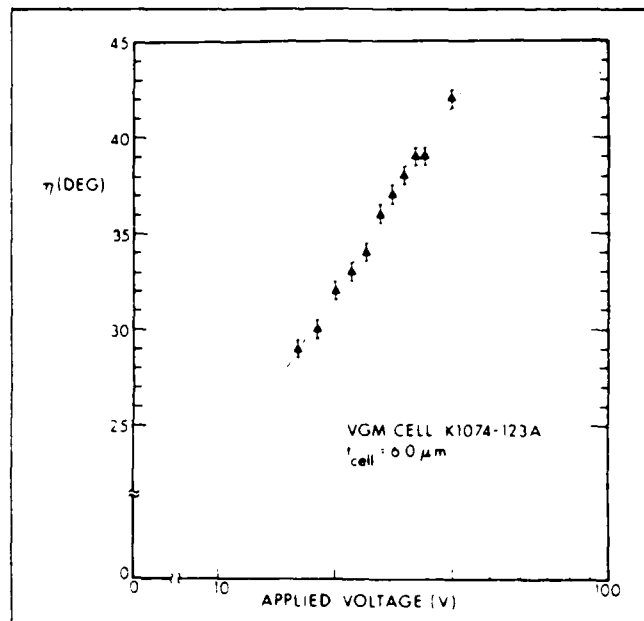


Fig. 13. The out-of-plane molecular orientation angle ( $\eta_0$ ) as a function of the applied dc bias voltage across the cell (V) (see Fig. 5).

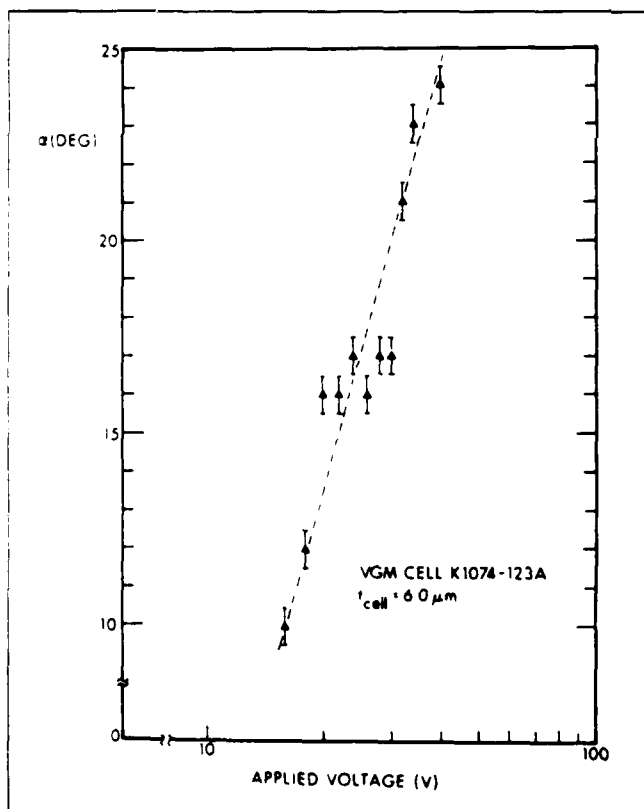


Fig. 12. The in-plane molecular orientation angle ( $\alpha_0$ ) as a function of the applied dc bias voltage across the cell (V) (see Fig. 5).

in which  $\epsilon^* = \epsilon_1 - \epsilon_3$ ,  $\mu = (\epsilon_a K / 4\pi\epsilon^2)$ , and  $\epsilon_a = \epsilon_e - \epsilon_o$ . The dispersion relation is linear when  $k \gg \pi/t$ , as shown in Fig. 15 (compare with the experimental relationship shown in Fig. 4).

The origin of the periodic instability in VGM liquid crystals has

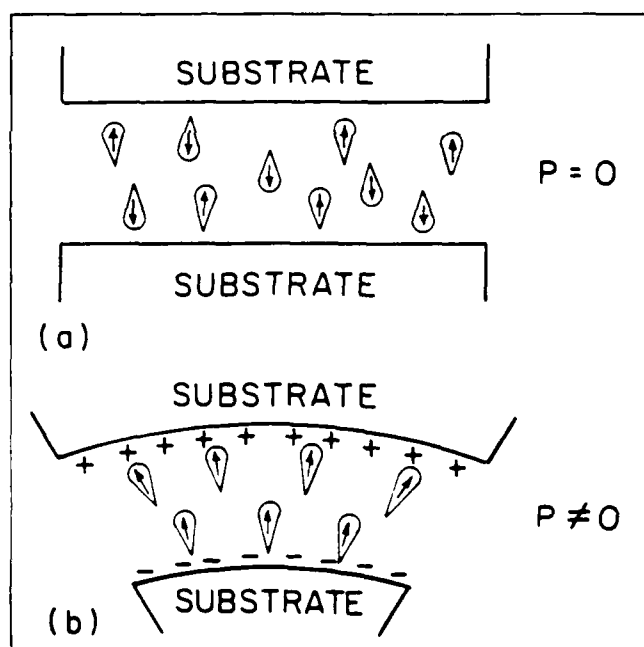


Fig. 14. Schematic diagram illustrating a possible mechanism for the occurrence of the flexoelectric effect due to a shape anisotropy in liquid crystal molecules with a permanent dipole moment. In (a), the molecular orientations are randomly distributed, resulting in zero net polarization. In (b), the applied distortion induces a shape-dependent molecular realignment, resulting in a net polarization. (After Ref. 31.)

not yet been established beyond doubt, although the accumulated evidence points strongly toward the converse flexoelectric effect. This assignment is also intuitively appealing since the VGM effect is observed only in liquid crystal mixtures with slightly negative dielectric anisotropy,<sup>12</sup> for which both the dielectric and distortion contributions to the free energy *increase* for deviations from uniform alignment. The addition of the flexoelectric term counteracts these

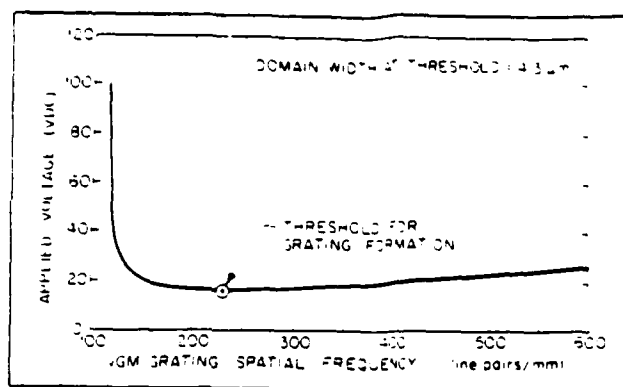


Fig. 18. Resultant theoretical dispersion relation for liquid crystal parameters corresponding to HRL 2N40 phenyl benzoate mixture (see Eq. (7)), subject to the assumption that  $K_1 = K_2 = K$ .

effects, producing a free-energy minimum at nonzero distortion angles. Furthermore, this model predicts a static periodic perturbation; no hydrodynamic or electrohydrodynamic effects are observed in our test cells.

The dynamics of grating formation, reorientation, and relaxation are subjects of ongoing experimental and theoretical investigation. Understanding of the basic physical principles underlying these effects is vital to the success of efforts to improve the VGM LCD response time.

A number of spatial discontinuities which are similar in appearance to crystallographic dislocations can be observed within the liquid crystal layer (see Fig. 7). The "dislocation" density increases with time as each VGM device deteriorates, and strongly depends on the manner in which the applied bias is brought from below to above the threshold of grating formation. In some cases, as the applied bias across an electrically activated cell is increased or decreased, the dislocations propagate past each other while the grating period decreases or increases, respectively. Dislocations with opposite orientations propagate in opposite directions until a new stable equilibrium situation is achieved. It is not yet clear whether these dislocations represent true disclinations, for which the liquid crystal director is discontinuous near the defect, or whether they are in fact alternative local continuous solutions to the free-energy minimization, perhaps induced by an as yet undiscovered perturbation.

A large number of research directions have been described in the foregoing paragraphs. In addition, several others are worthy of note. First, numerous experimental measurements of the off-diagonal elements in the Jones matrix describing polarized light propagation through the VGM cell have revealed a significant asymmetry not predicted by the uniaxial model. The origin of this "B/C" asymmetry effect has not yet been elucidated. Second, the thickness dependence of the molecular orientation angles  $\alpha$  and  $\eta$  has not been fully established. The solution proposed<sup>21</sup> in Eq. (6) assumes full surface pinning at the substrate boundaries, and represents the lowest order z-dependent mode. The polarization-dependent diffracted order measurements described herein do not provide clear differentiation between a uniform z-dependence and the lowest order mode. Third, the nature of the transient solutions to the free-energy minimization incorporating molecular dynamic and viscosity effects has not been treated. Solution of this problem is key to response time optimization of the VGM liquid crystal device. Fourth, it is not yet clear whether a nematic liquid crystal mixture can be found that exhibits a useful VGM effect under ac bias. Such a mixture may provide significant immunity from long-term ion-poisoning effects. Finally, it should be emphasized that the variable grating mode liquid crystal effect provides

only one possible means of achieving parallel intensity-to-position encoding. The processing potential of the intensity-to-position algorithm should provide more than adequate inducement to intensify the search for alternative implementations.

## 5. ACKNOWLEDGMENTS

The authors gratefully acknowledge the contributions of D. Boswell, A. M. Lackner, and J. D. Margerum (Hughes Research Laboratories), and K. Sherman and G. Edwards (University of Southern California). This research was supported by the U.S. Air Force Office of Scientific Research, Electronics and Solid State Sciences Division, under grant AFOSR-81-0082 at the University of Southern California and contract F49620-81-C-0086 at Hughes Research Laboratories.

## 6. REFERENCES

1. R. V. Johnson, D. L. Hecht, R. A. Sprague, L. N. Flores, D. L. Steinmetz, and W. D. Turner, *Opt. Eng.* 22(6), 665 (1983).
2. D. L. Pape and L. J. Hornbeck, *Opt. Eng.* 22(6), 675 (1983).
3. U. Efron, P. O. Braatz, M. J. Little, R. N. Schwartz, and J. Grinberg, *Opt. Eng.* 22(6), 682 (1983).
4. C. Warde and J. Thackara, *Opt. Eng.* 22(6), 695 (1983).
5. D. Casasent, *Proc. IEEE* 65, 143 (1977).
6. S. Lipson, "Recyclable Incoherent-to-Coherent Image Converters," in *Advances in Holography*, N. Farhat, Ed., Marcel Dekker, New York (1979).
7. G. Knight, "Interface Devices and Memory Materials," in *Optical Data Processing*, S. H. Lee, Ed., Springer-Verlag, Heidelberg (1976).
8. A. R. Tanguay, Jr., *Proc. ARO Workshop on Future Directions for Optical Information Processing*, Texas Tech University, Lubbock, Texas, 52(1980).
9. B. H. Soffer, D. Boswell, A. M. Lackner, A. R. Tanguay, Jr., T. C. Strand, and A. A. Sawchuk, in *Devices and Systems for Optical Signal Processing*, T. C. Strand and A. R. Tanguay, Jr., Eds., *Proc. SPIE* 218, 81 (1980).
10. B. H. Soffer, D. Boswell, A. M. Lackner, P. Chavel, A. A. Sawchuk, T. C. Strand, and A. R. Tanguay, Jr., in *1980 International Optical Computing Conference (Book II)*, *Proc. SPIE* 232, 128 (1980).
11. P. Chavel, A. A. Sawchuk, T. C. Strand, A. R. Tanguay, Jr., and B. H. Soffer, *Opt. Lett.* 5, 398 (1980).
12. B. H. Soffer, J. D. Margerum, A. M. Lackner, D. Boswell, A. R. Tanguay, Jr., T. C. Strand, A. A. Sawchuk, and P. Chavel, *Mol. Cryst. Liq. Cryst.* 70, 145 (1981).
13. A. R. Tanguay, Jr., submitted for publication in *Opt. Lett.*
14. A. R. Tanguay, Jr., P. Chavel, T. C. Strand, C. S. Wu, and B. H. Soffer, submitted for publication in *Opt. Lett.*
15. J. B. Margerum, J. E. Jensen, and A. M. Lackner, *Mol. Cryst. Liq. Cryst.* 68, 137 (1981).
16. W. Greubel and U. Wolff, *Appl. Phys. Lett.* 19(7), 213 (1971).
17. J. W. Goodman, *Introduction to Fourier Optics*, McGraw-Hill, New York (1968).
18. B. H. Soffer, "Real-Time Implementation of Nonlinear Optical Processing Functions," Annual Technical Report on AFOSR F49620-81-C-0086, (1982).
19. R. B. Meyer, *Phys. Rev. Lett.* 22(18), 918 (1969).
20. A. I. Derzhanski, A. G. Petrov, Ch. P. Khinov, and B. L. Markovski, *Bulg. J. Phys.* 2, 165 (1974).
21. Yu. P. Bobylev and S. A. Pikin, *Sov. Phys. JETP* 45(1), 195 (1977).
22. Yu. P. Bobylev, V. G. Chignov, and S. A. Pikin, *J. de Phys.* 40, Suppl. 4, C3-331 (1979).
23. S. A. Pikin, *Mol. Cryst. Liq. Cryst.* 63, 181 (1981).
24. J. M. Pollack and J. B. Flannery, *Society for Information Display 1976 Intern. Symp. Digest*, 143 (1976).
25. J. M. Pollack and J. B. Flannery, in *Liquid Crystals and Ordered Fluids*, J. F. Johnson and R. E. Porter, Eds., Vol. 2, pp. 557-571, Plenum Press, New York (1974).
26. J. M. Pollack and J. B. Flannery, in *Liquid Crystals and Ordered Fluids*, J. F. Johnson and R. E. Porter, Eds., Vol. 3, pp. 421-442, Plenum Press, New York (1978).
27. L. K. Vistin, *Sov. Phys.-Dokl.* 15(10), 908 (1971).
28. L. K. Vistin, *Sov. Phys.-Crystallogr.* 15(3), 514 (1970).
29. A. Derzhanski, A. G. Petrov, and M. D. Mitov, *J. de Phys.* 39, 273 (1978).
30. M. I. Barnik, L. M. Blinov, A. N. Trufanov, and B. A. Umanski, *J. de Phys.* 39, 417 (1978).
31. P. G. de Gennes, *The Physics of Liquid Crystals*, pp. 97-101, Oxford University Press, London (1974).
32. J. Prost and J. P. Marcerou, *J. de Phys.* 38, 315 (1977).
33. J. Prost and P. S. Pershan, *J. Appl. Phys.* 47, 2298 (1976).

END

FILMED

4-84

DTIC